Recent Modifications of Hydrothermal Diamond-anvil Cell and its Applications

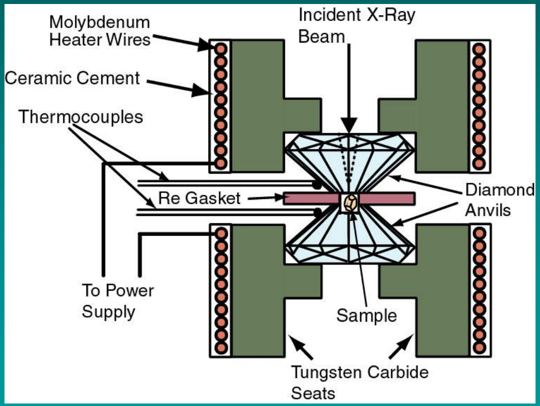

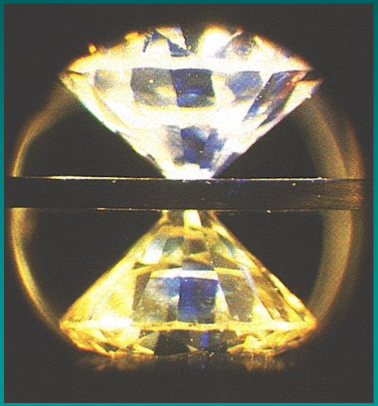

I-Ming Chou

Chinese Academy of Sciences,

Sanya Inst. of Deep-sea Sci. & Engineering

Lab for Experimental Study under Deep-sea Extreme Conditions

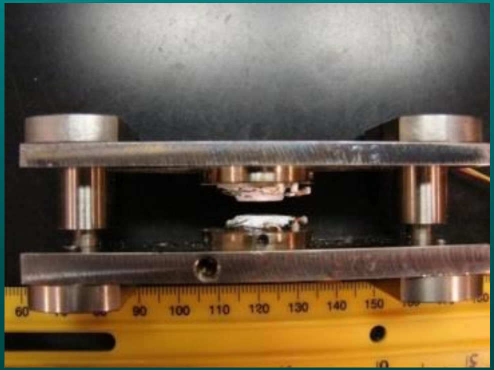

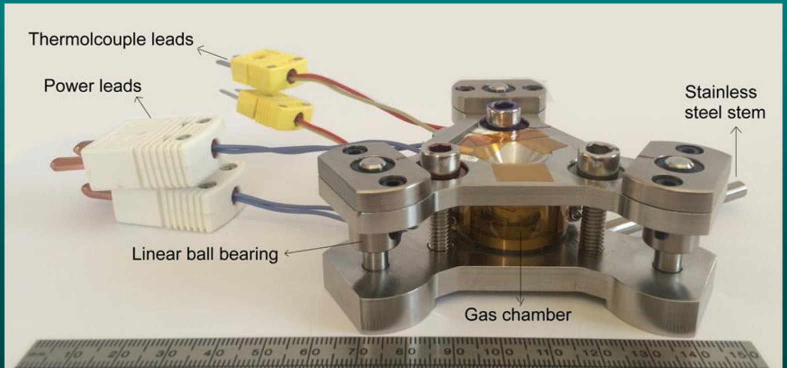

Outline

- About HDAC
- About SIDSSE
- Pressure measurements in HDAC
- Applications (Examples):
  - The system $KAlSi_3O_8$-H_2O
  - XAFS & structure of hydrothermal solutions
  - T_h measurements in FIs under elevated external pressures in HDAC
- Summary & Future Works

Hydrothermal Diamond Anvil Cell

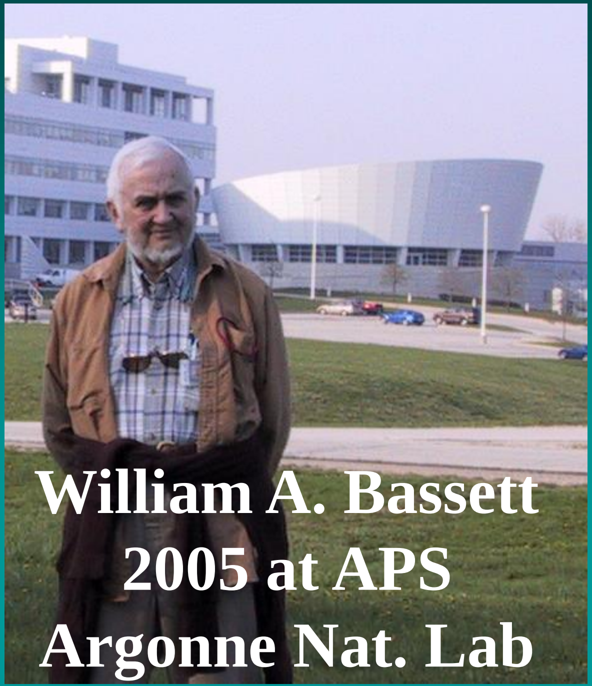

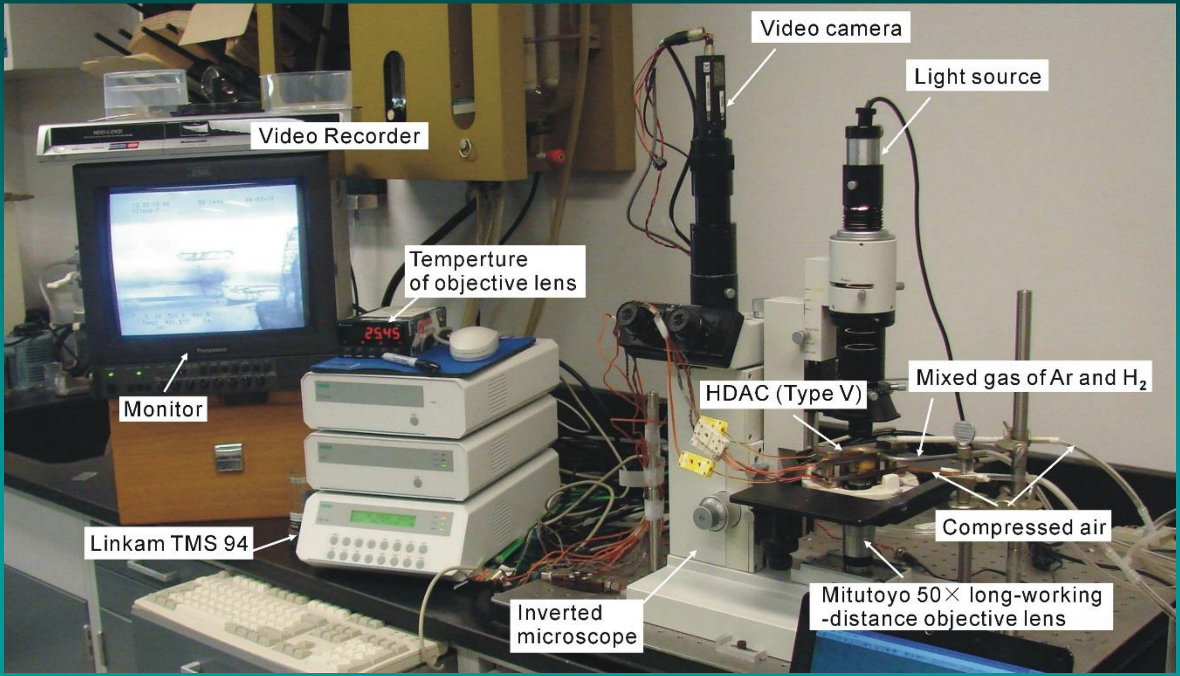

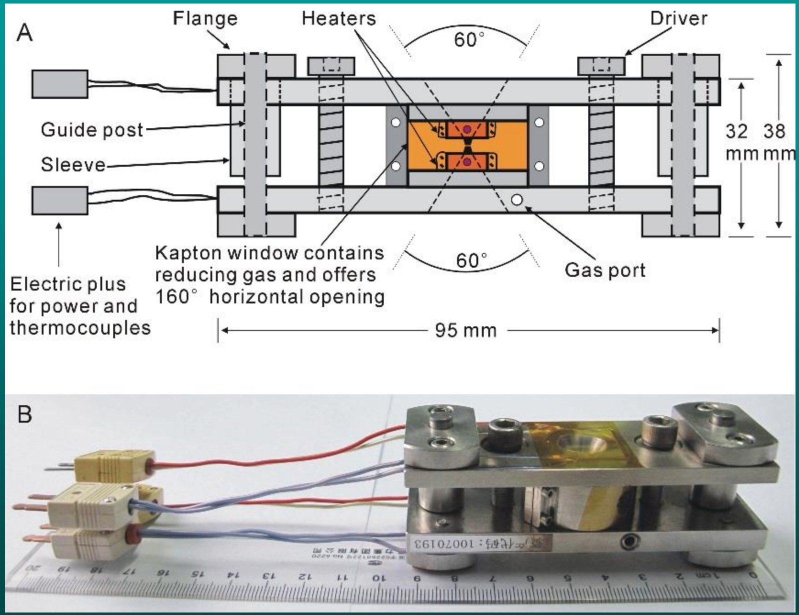

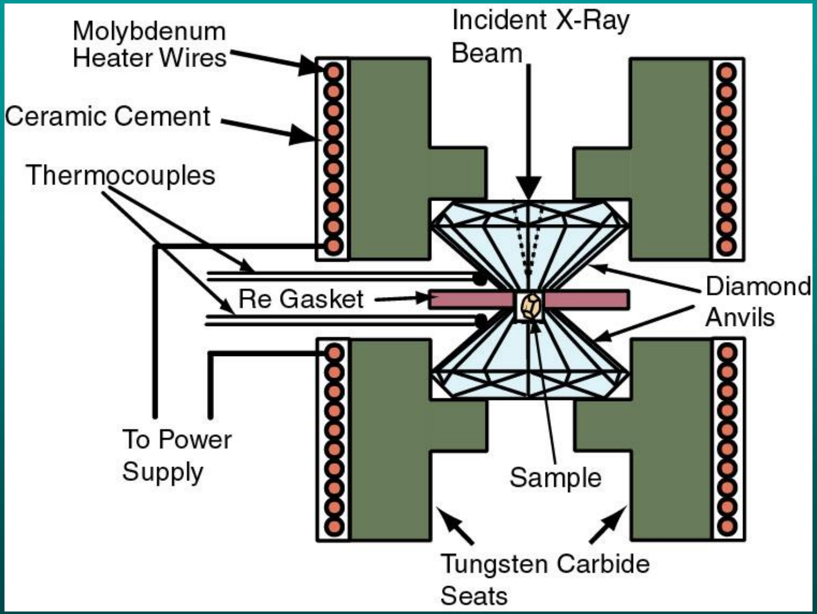

AIP | Review of Scientific Instruments

An improved hydrothermal diamond anvil cell

Jiankang Li, W. A. Bassett, I-Ming Chou, Xin Ding, Shenghu Li, and Xinyan Wang

Citation: Review of Scientific Instruments **87**, 053108 (2016); doi: 10.1063/1.4947506

View online: http://dx.doi.org/10.1063/1.4947506

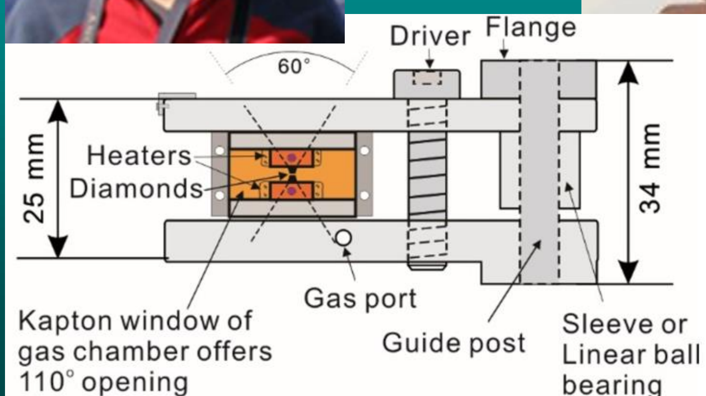

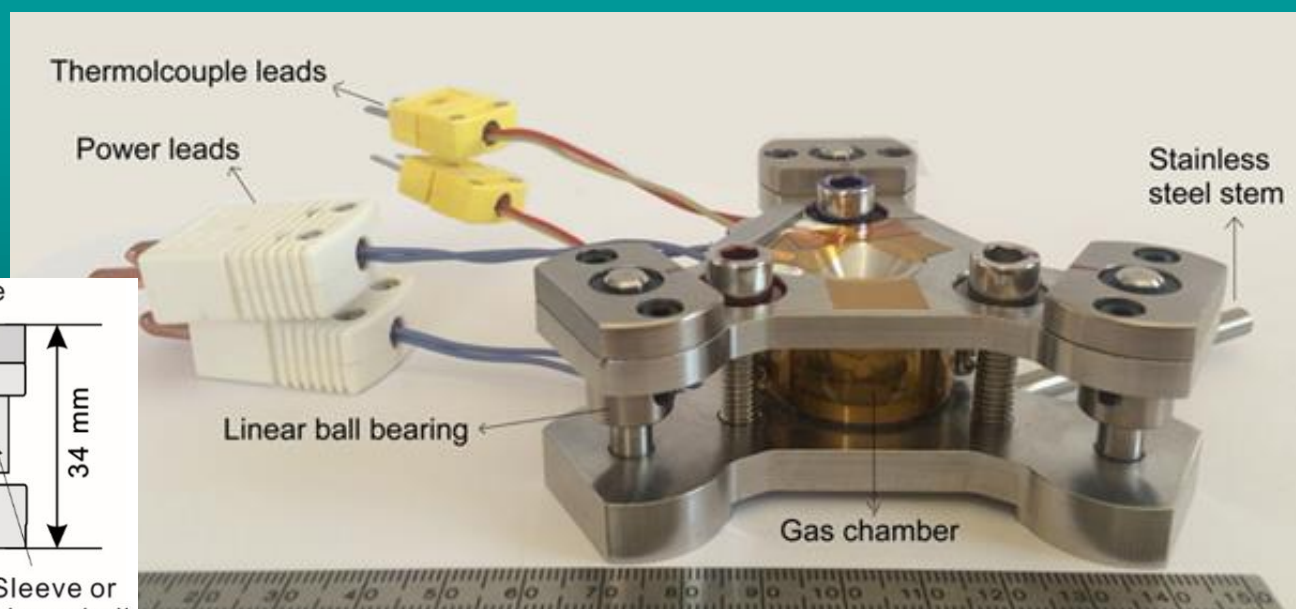


Hailar
Qiqihar
Karamay
Yining
Urumqi
MONGOLIA
Cherlen Gol
Harbin
Changchun
Kashgar
Yumen
Hohhot
Beijing
Shenyang
KOREA
Tianjin
Yinchuan
Shijiazhuang
Golmud
Xining
Lanzhou
Taiyuan
Jinan
Yellow River
Yellow Sea
Shiquanhe
Zhengzhou
Xian
Nanjing
Hefei
Shanghai
Yarlong Tsangpo River
Chengdu
Yangtze River
Chongqing
Hangzhou
East China Sea
Lhasa
Nanchang
INDIA
Guiyang
Changsha
Fuzhou
Ganga
Brahmaputra
Kunming
Taibei
Guangzhou
BURMA
Nanning
Macau
Hong Kong
Dongsha Qundao
Haikou
Hainan
Sanya
Xisha Qundao
PHILIPPINES
Zhongsha Qundao
Mekong
South China Sea
sunnysanya

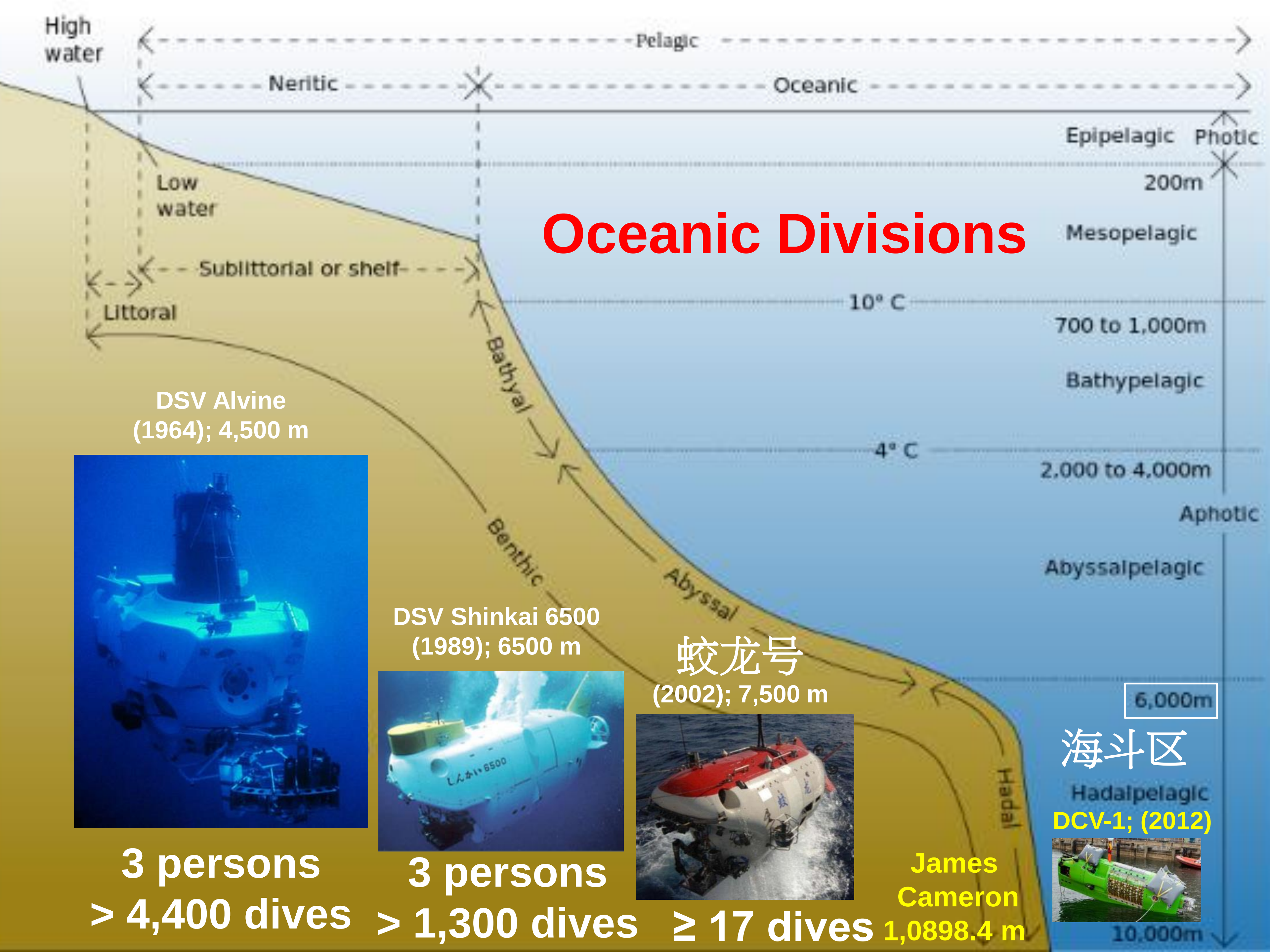
Oceanic Divisions
High water
Pelagic
Neritic
Oceanic
Epipelagic
Photic
200m
Low water
Mesopelagic
Sublittorial or shelf
Littoral
10° C
700 to 1,000m
Bathyal
Bathypelagic
4° C
2,000 to 4,000m
Aphotic
Benthic
Abyssal
Abyssalpelagic
6,000m
Hadal
海斗区
Hadalpelagic
10,000m
DSV Alvine
(1964); 4,500 m
3 persons
> 4,400 dives
DSV Shinkai 6500
(1989); 6500 m
3 persons
> 1,300 dives
蛟龙号
(2002); 7,500 m
≥ 17 dives
James
Cameron
1,0898.4 m
DCV-1; (2012)

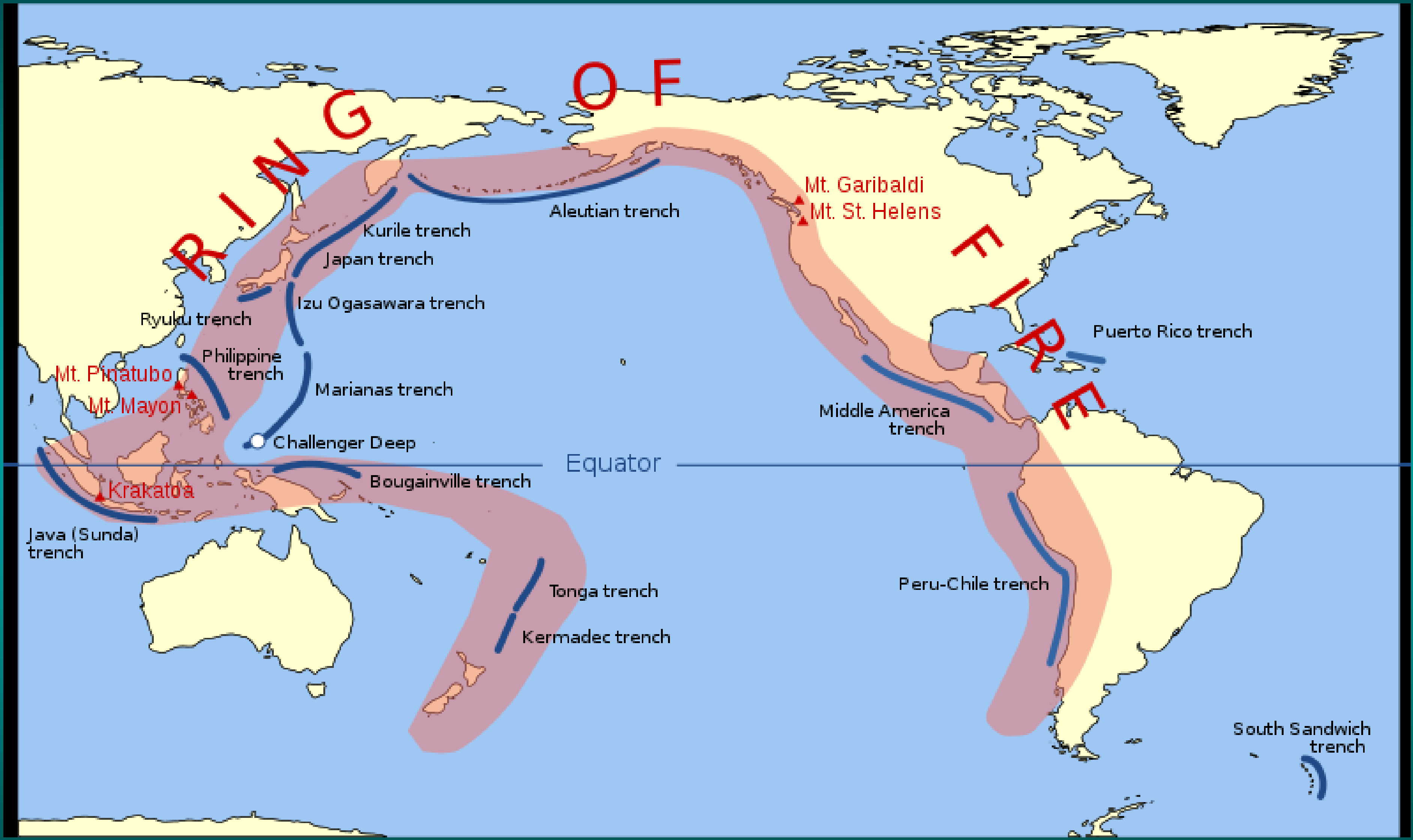

RING OF FIRE
Aleutian trench
Kurile trench
Japan trench
Izu Ogasawara trench
Ryuku trench
Philippine trench
Marianas trench
Challenger Deep
Mt. Pinatubo
Mt. Mayon
Krakatoa
Java (Sunda) trench
Bougainville trench
Equator
Tonga trench
Kermadec trench
Mt. Garibaldi
Mt. St. Helens
Puerto Rico trench
Middle America trench
Peru-Chile trench
South Sandwich trench

Tectonic setting of the Tonga–Kermadec arc/back-arc system

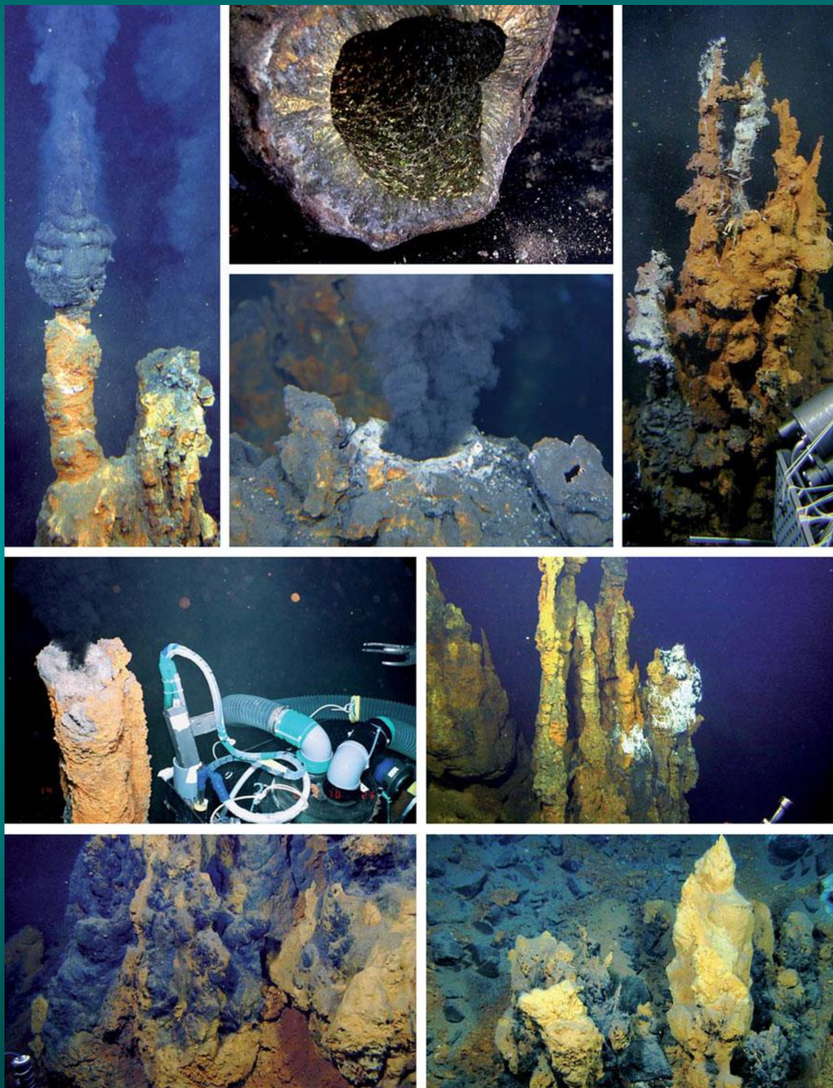

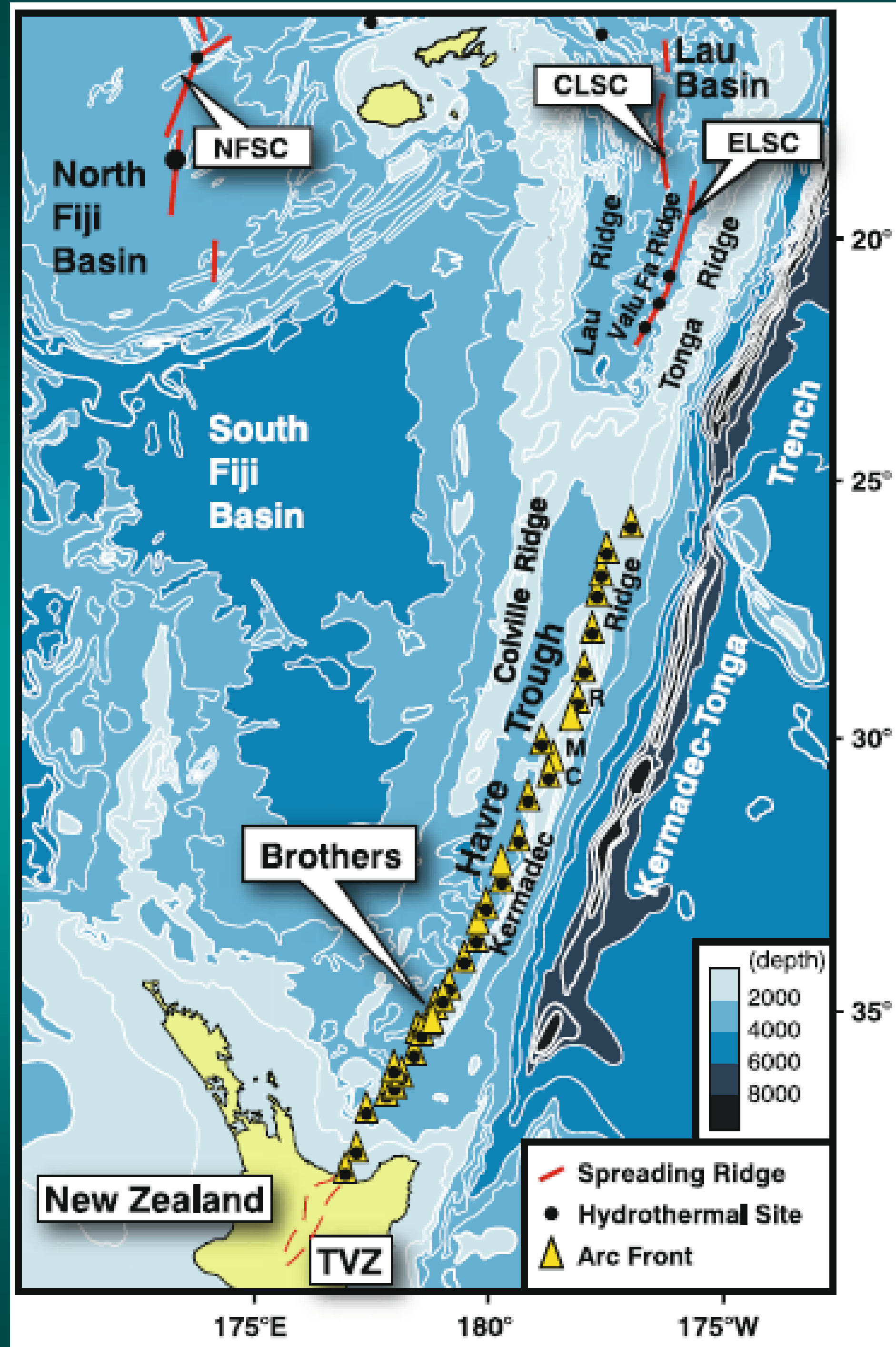

A cartoon showing
submarine hydrothermal activities
at Brothers Volcano
Kermadec Arc
New Zealand

De Ronde et al. (2011)
Mineralium Deposita
46:541-584

A total of nine dives were made:
four by Shinkai 6500 and
five by Pisces V.

High-pressure cells constructed with
fused silica capillary tubes are ideal
for the study of submarine hydrothermal
reactions for fluids containing
C, O, H, and S.

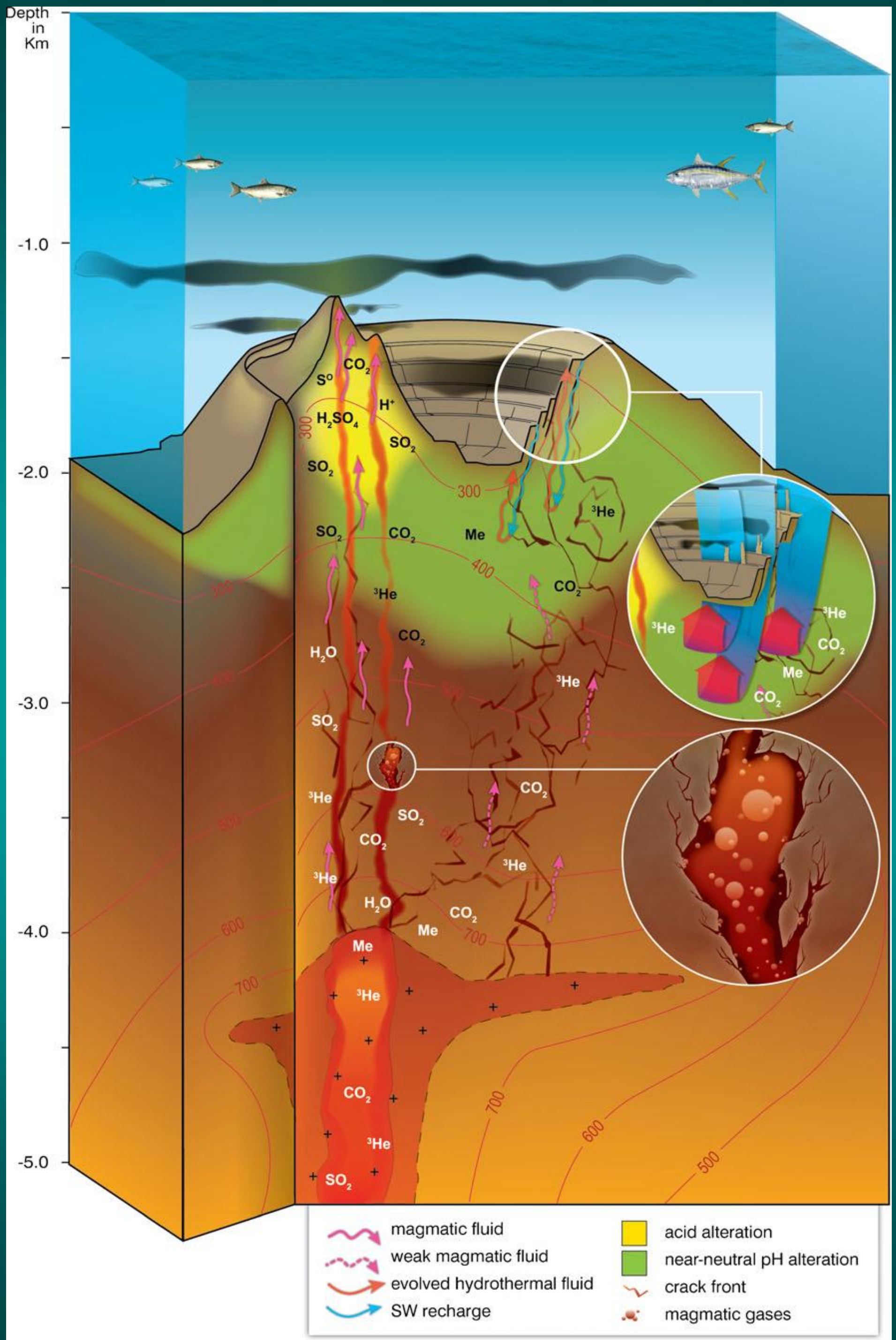

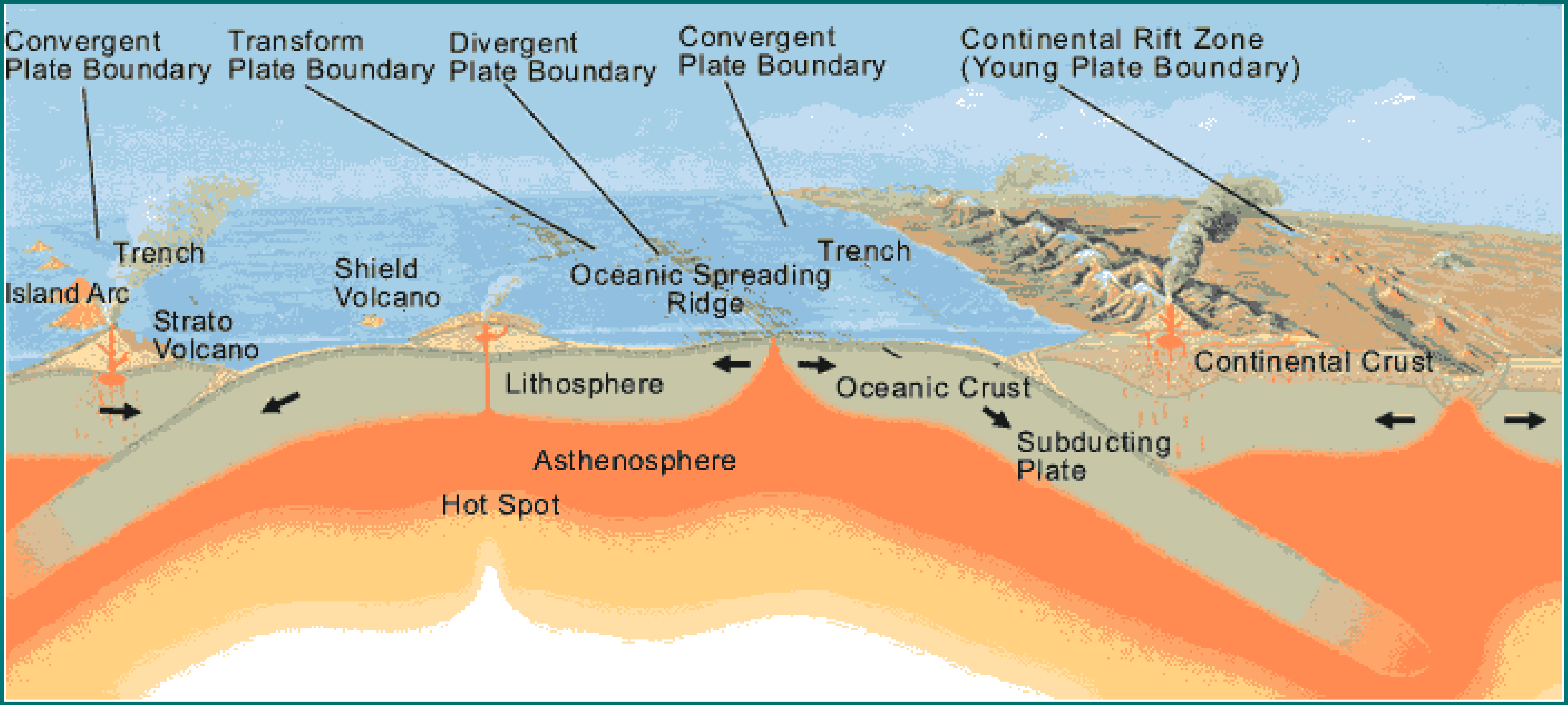

Convergent
Plate Boundary
Transform
Plate Boundary
Divergent
Plate Boundary
Convergent
Plate Boundary
Continental Rift Zone
(Young Plate Boundary)
Trench
Island Arc
Strato
Volcano
Shield
Volcano
Oceanic Spreading
Ridge
Trench
Continental Crust
Lithosphere
Oceanic Crust
Subducting
Plate
Asthenosphere
Hot Spot

SIDSSE Resarch on Extraterrestrial Oceans

91 x 48 km

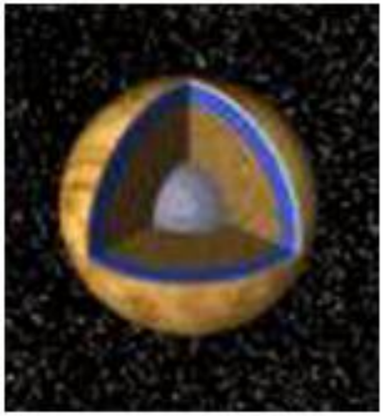

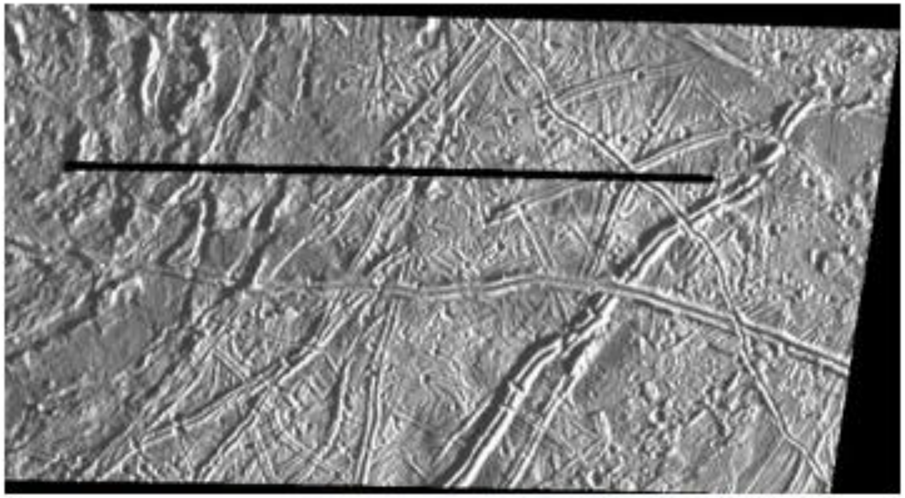

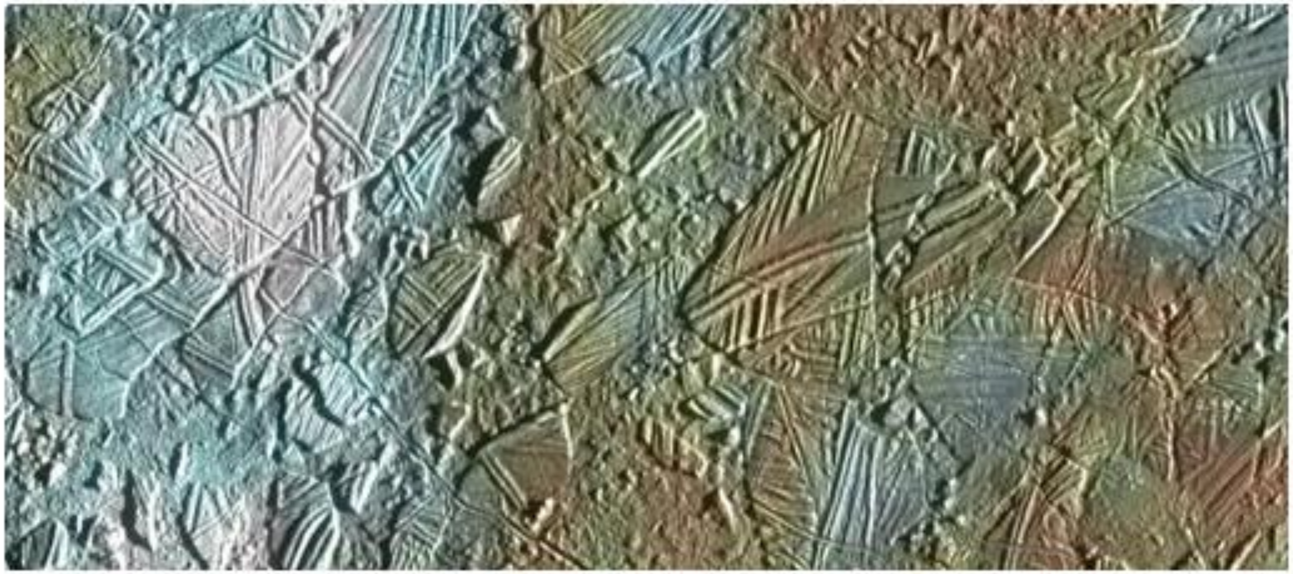

70 x 30 km

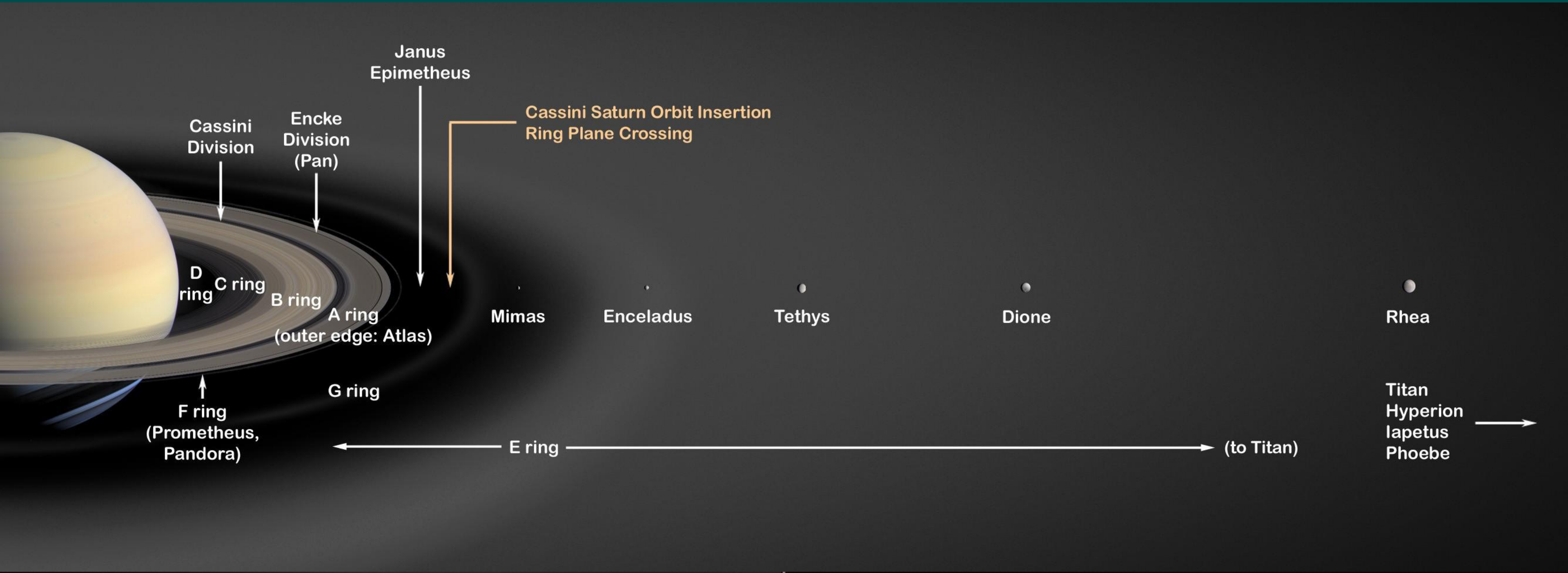
Janus
Epimetheus
Cassini Saturn Orbit Insertion
Ring Plane Crossing
Cassini
Division
Encke
Division
(Pan)
D
ring
C ring
B ring
A ring
(outer edge: Atlas)
Mimas
Enceladus
Tethys
Dione
Rhea
G ring
F ring
(Prometheus,
Pandora)
E ring
(to Titan)
Titan
Hyperion
Iapetus
Phoebe

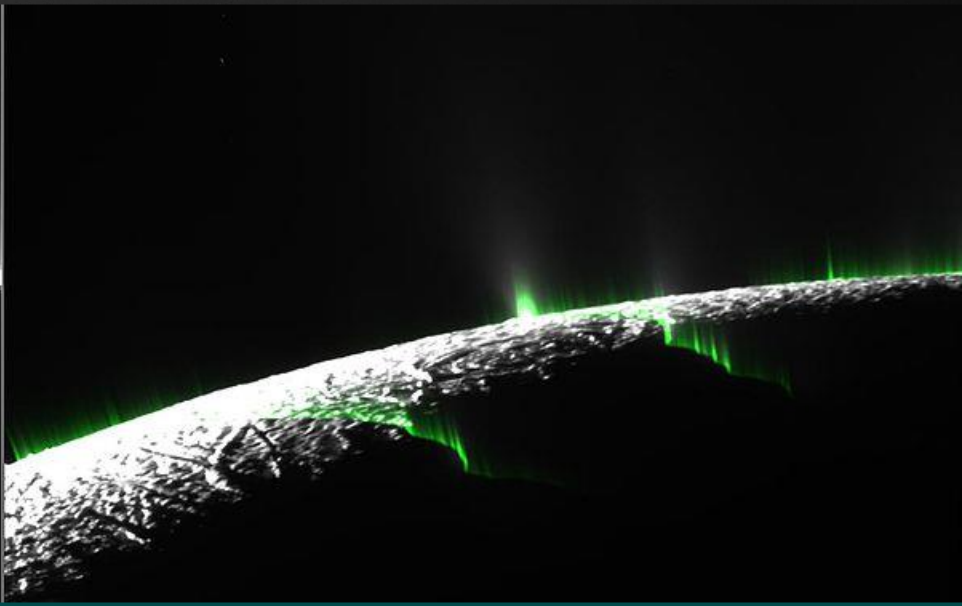

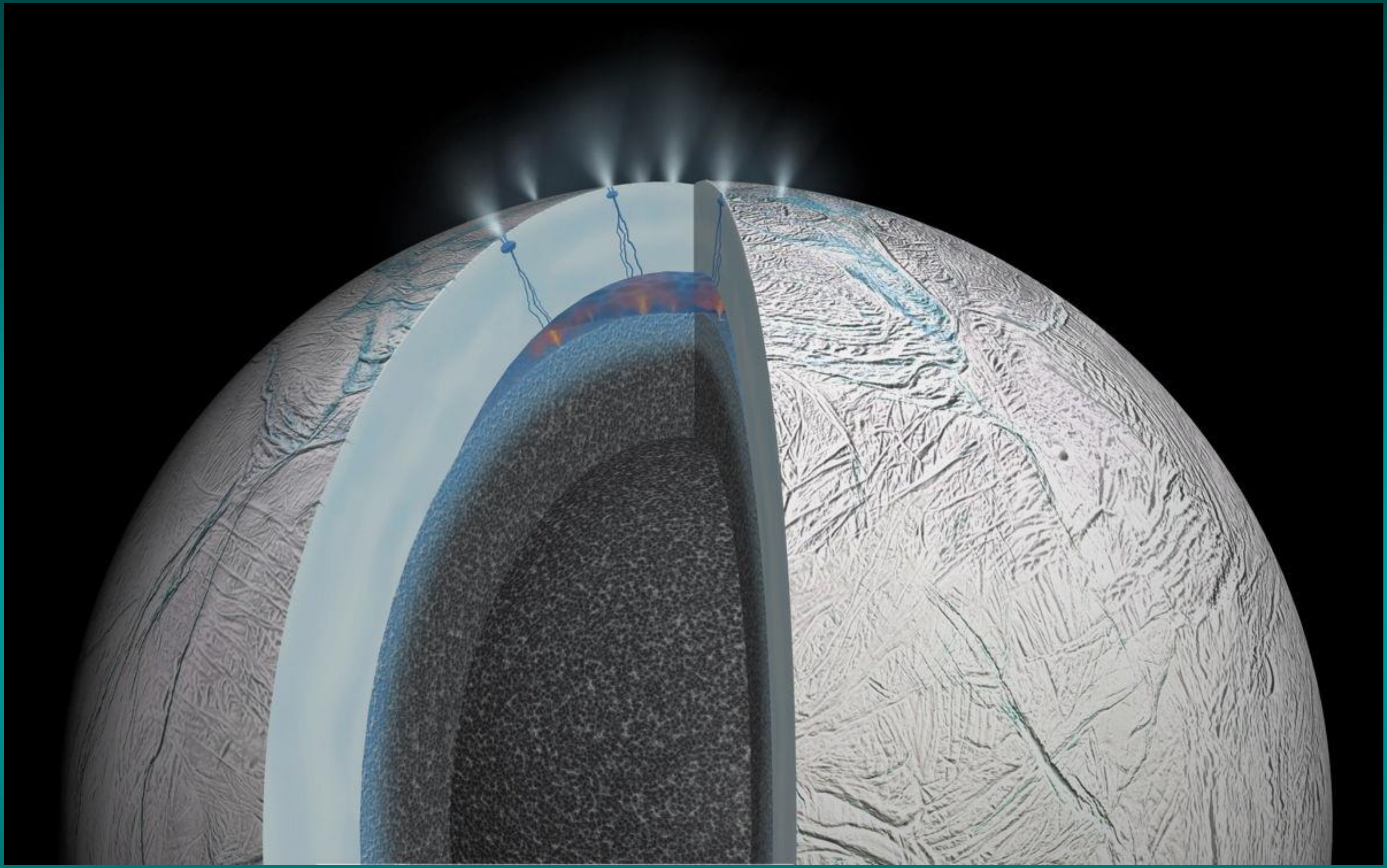

Salt-rich ice plums contain 4 to 16-nm silica grains: formed in solution > 90 ˚C; 40 km depth; pH > 8.5; salinity < 4% (3.2-3.7% for Earth seawater)

A schematic of Enceladus' interior

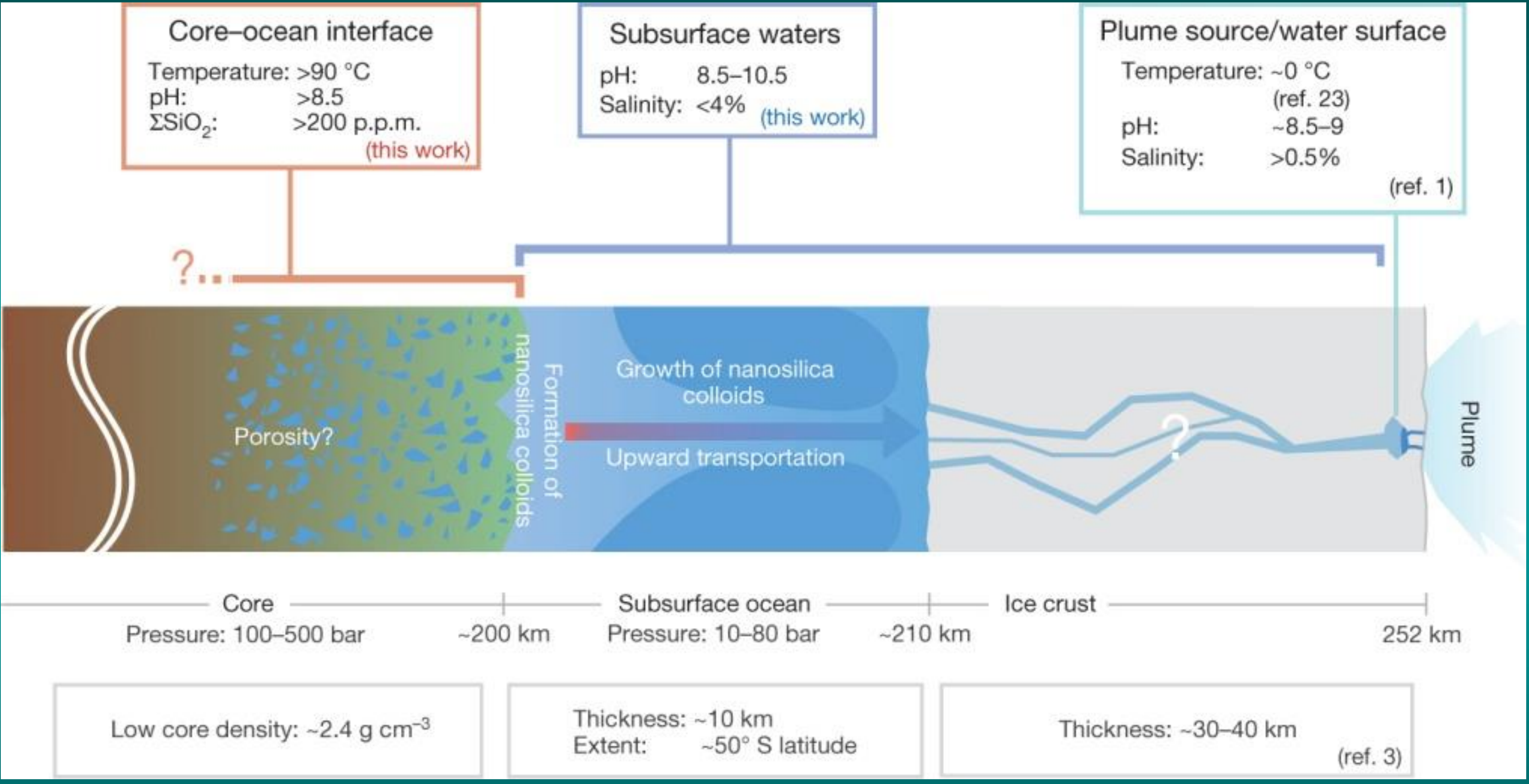

H-W Hsu *et al. Nature* 519, 207-210 (2015)
doi:10.1038/nature14262

nature

High pressure high temperature pressure vessels in SIDSSE

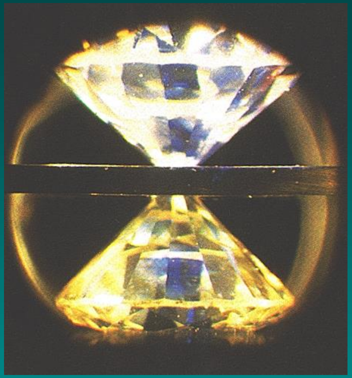

- (1) Hydrothermal Diamond-anvil cell
  - up to 50 kbar and 1000 ˚C
- (2) Fused silica capillary cell
  - up to 2 kbar and 600 ˚C

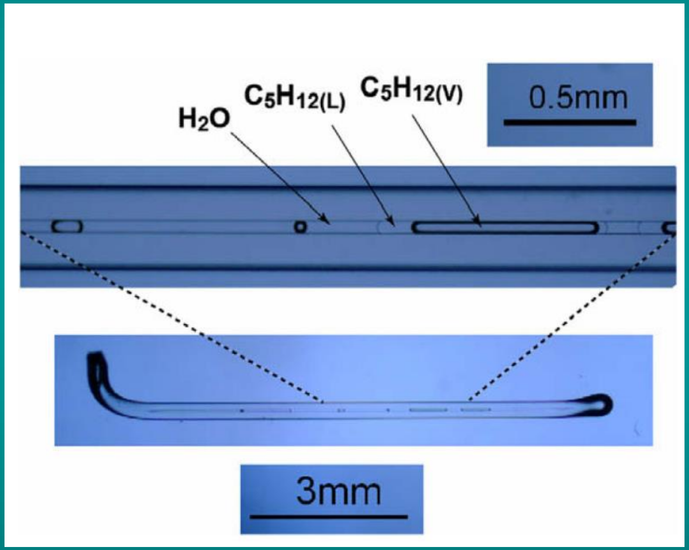

- (3) Cold-seal pressure vessel
  - up to to 2 kbar and 850 ˚C

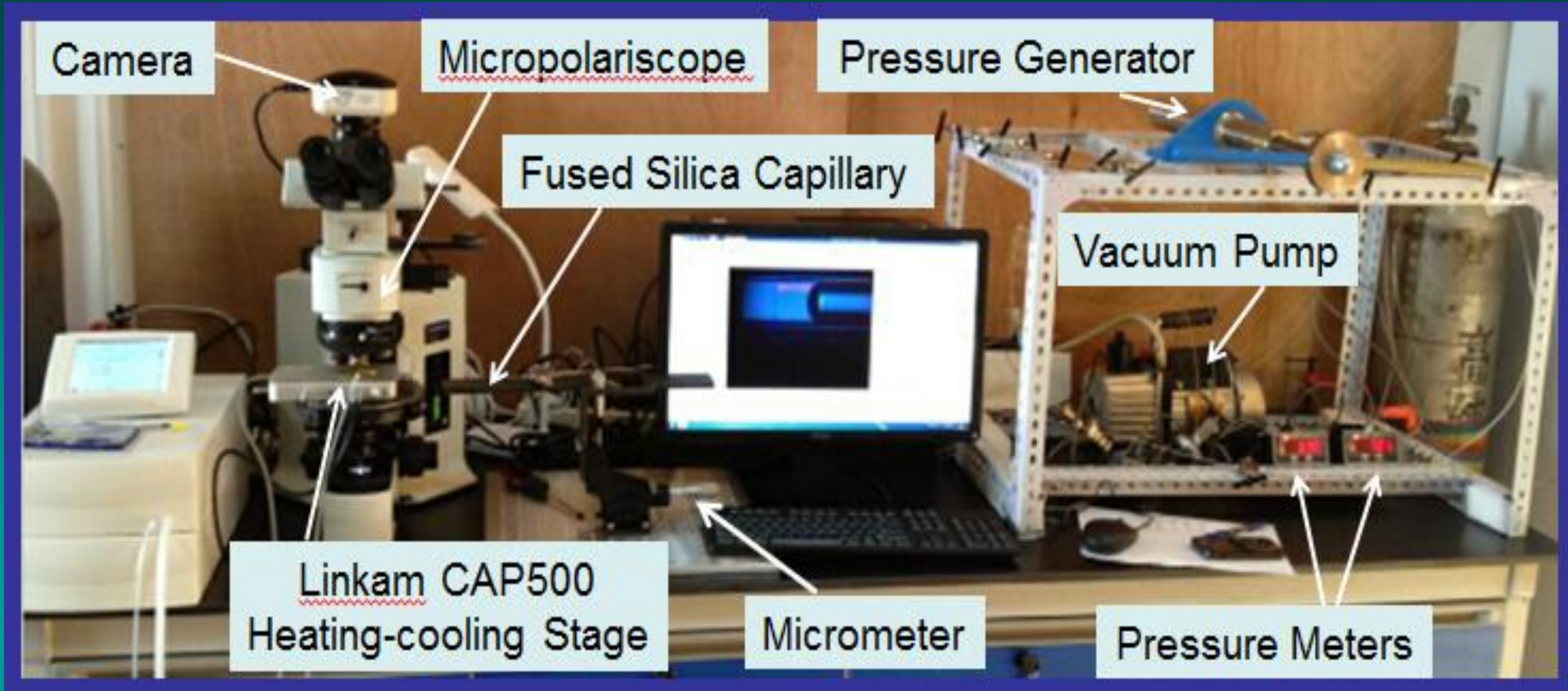
Camera
Micropolariscope
Pressure Generator
Fused Silica Capillary
Vacuum Pump
Linkam CAP500
Heating-cooling Stage
Micrometer
Pressure Meters
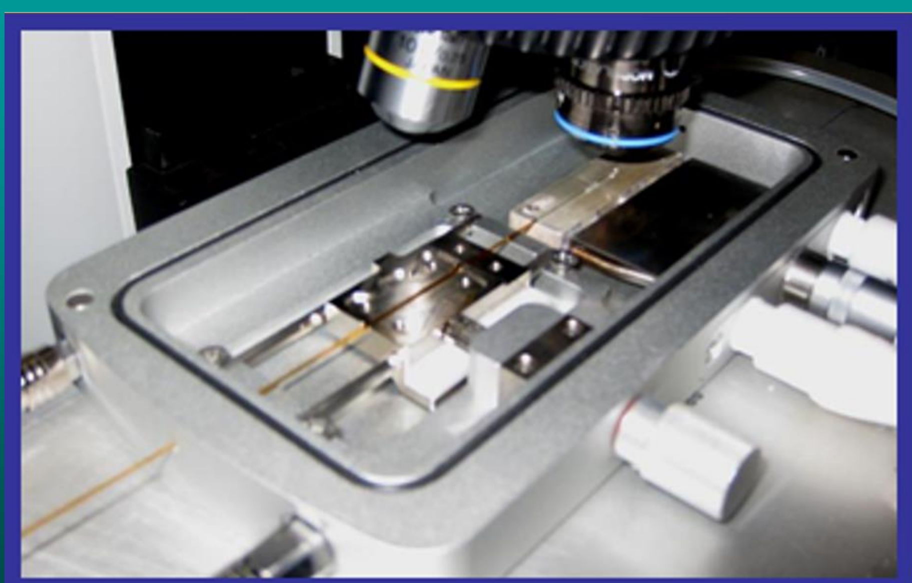



LabRAM HR Evolution
RAMAN SPECTROMETER
HORIBA
KIMMON

Monterey Bay Aquarium Research Institute

Pasteris et al. (2004)
Applied Spectroscopy
58: 195A-208A

(DORISS)
deep-ocean
Raman in situ
spectrometer
system

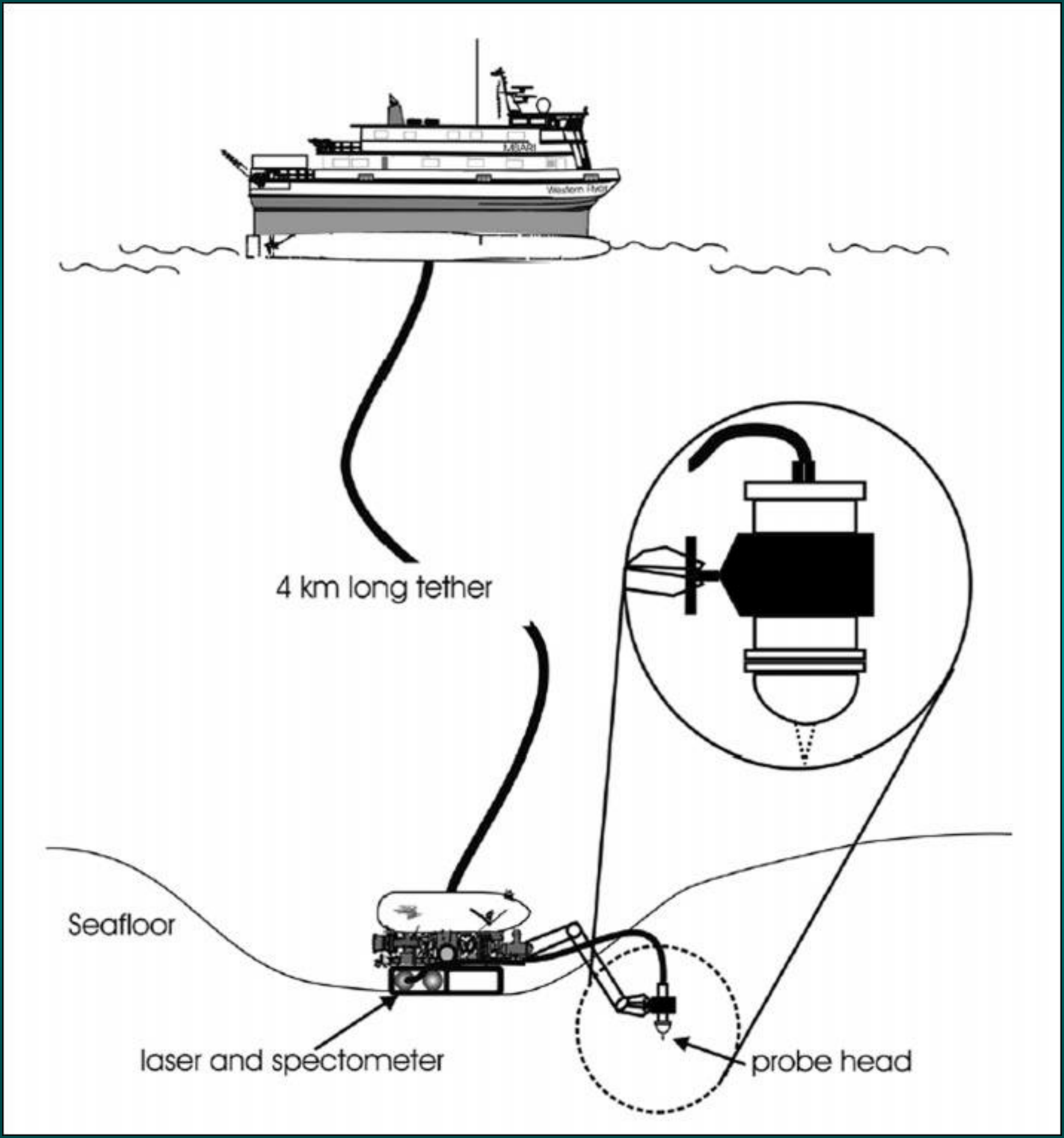

Hydrothermal Diamond Anvil Cell

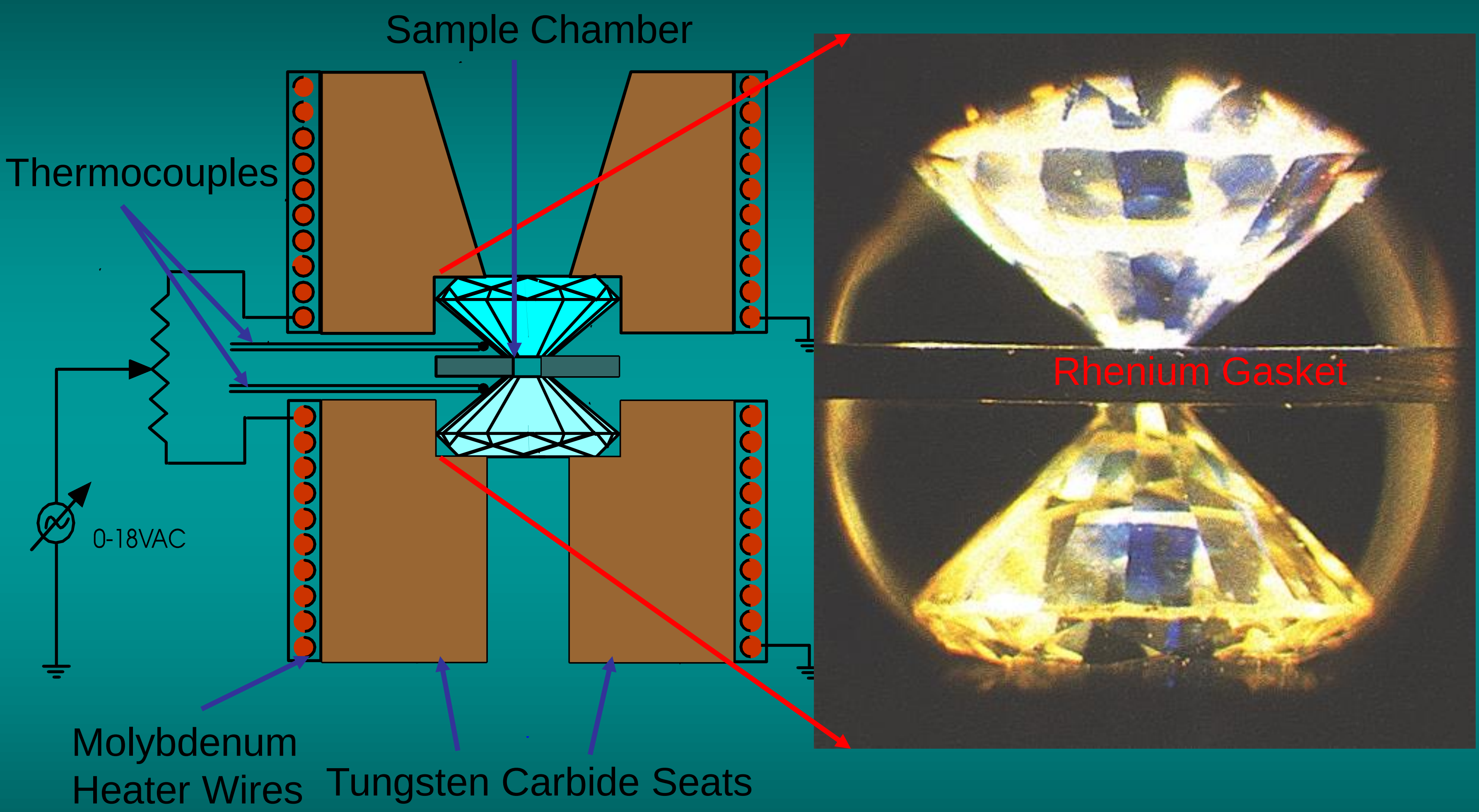

IN
1 2 3 4 5 6

铁橄榄石 + 石英 = 铁辉石

Fayalite + Qtz = Ferrosilite

($Fe_2SiO_4 + SiO_2 = 2\ FeSiO_3$)

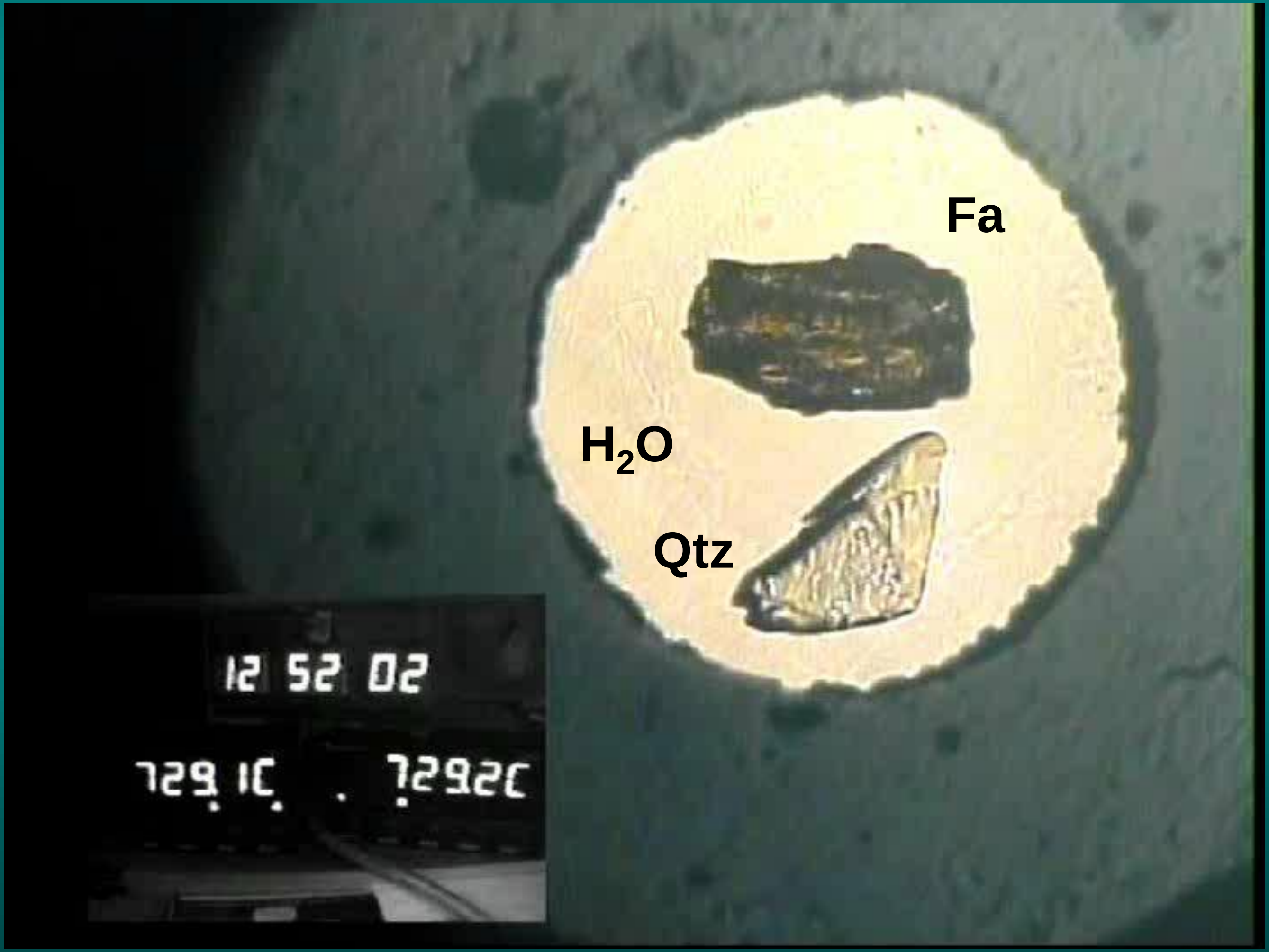

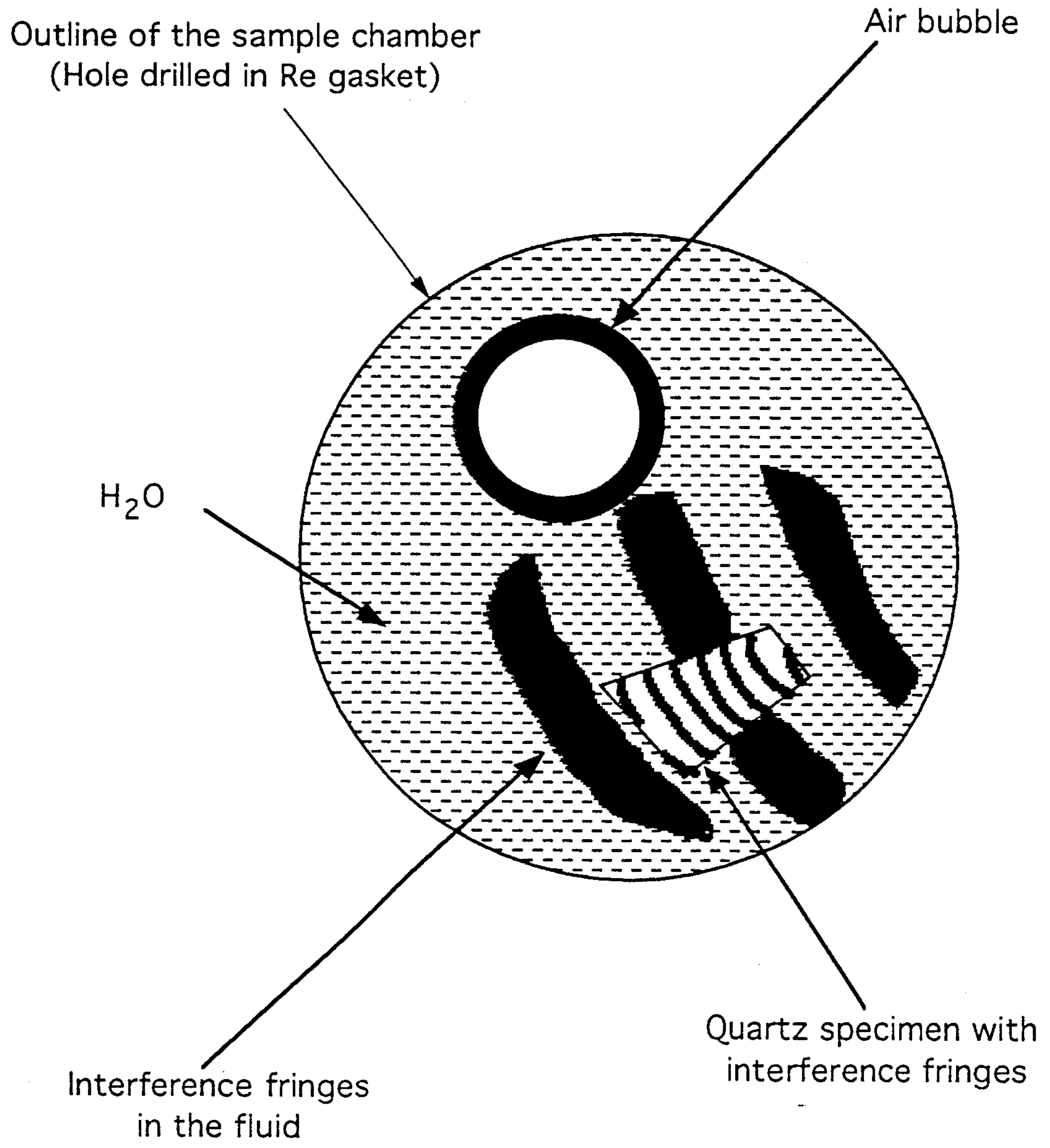

Outline of the sample chamber
(Hole drilled in Re gasket)
Air bubble
H_2O
Interference fringes
in the fluid
Quartz specimen with
interference fringes

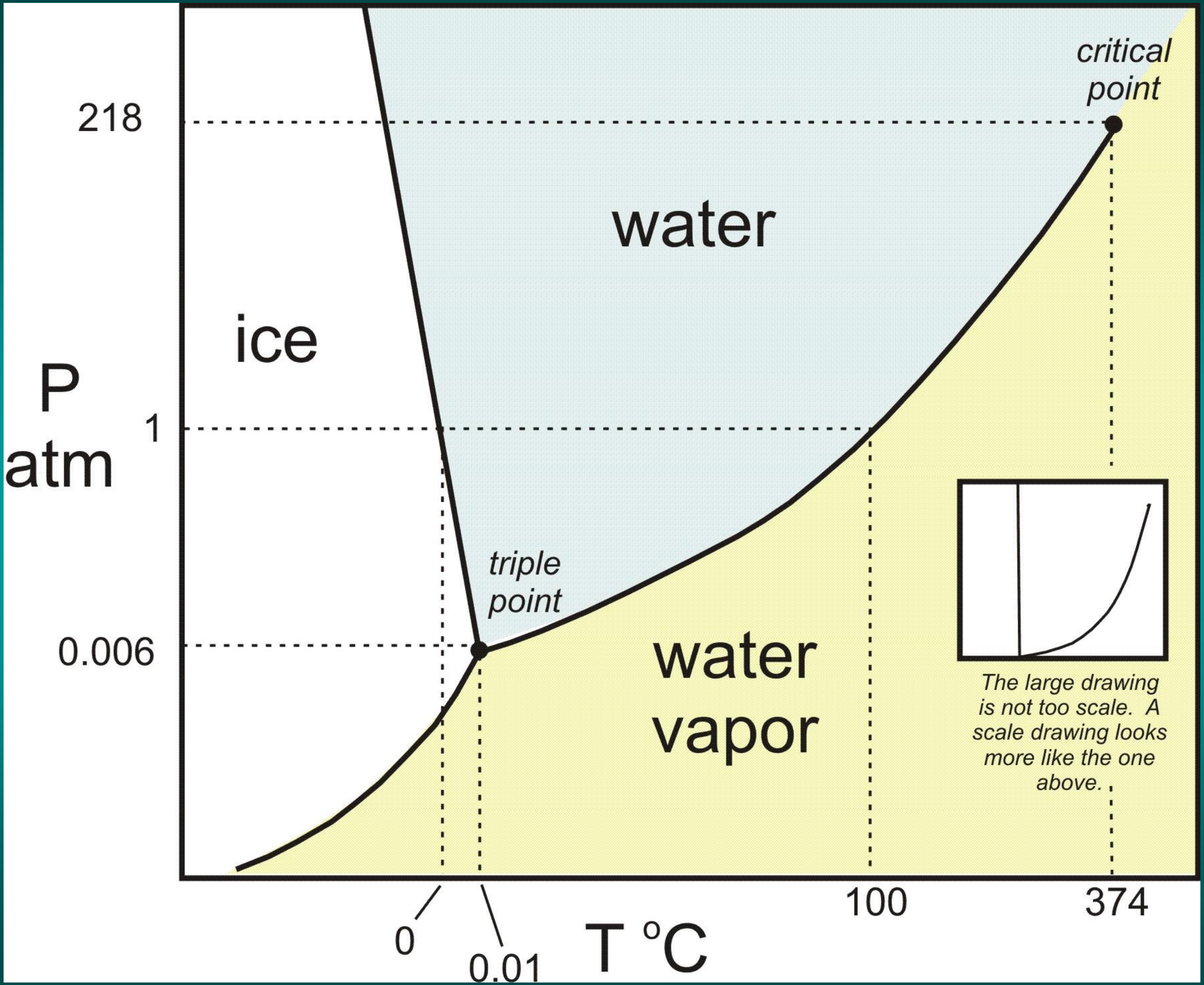
critical
point
218
water
ice
P
atm
1
triple
point
0.006
water
vapor
The large drawing is not too scale. A scale drawing looks more like the one above.
0
0.01
T °C
100
374

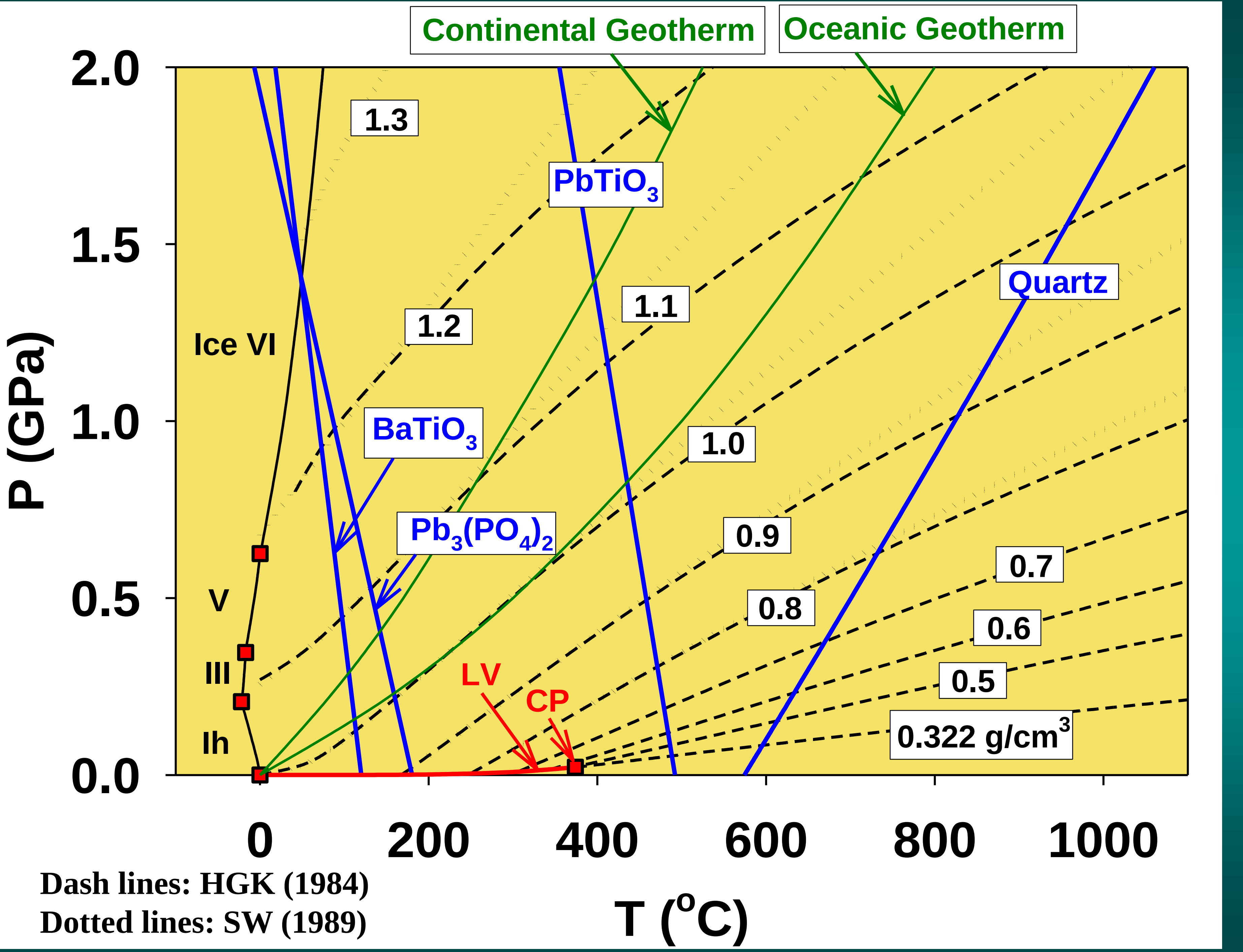

Dash lines: HGK (1984)
Dotted lines: SW (1989)

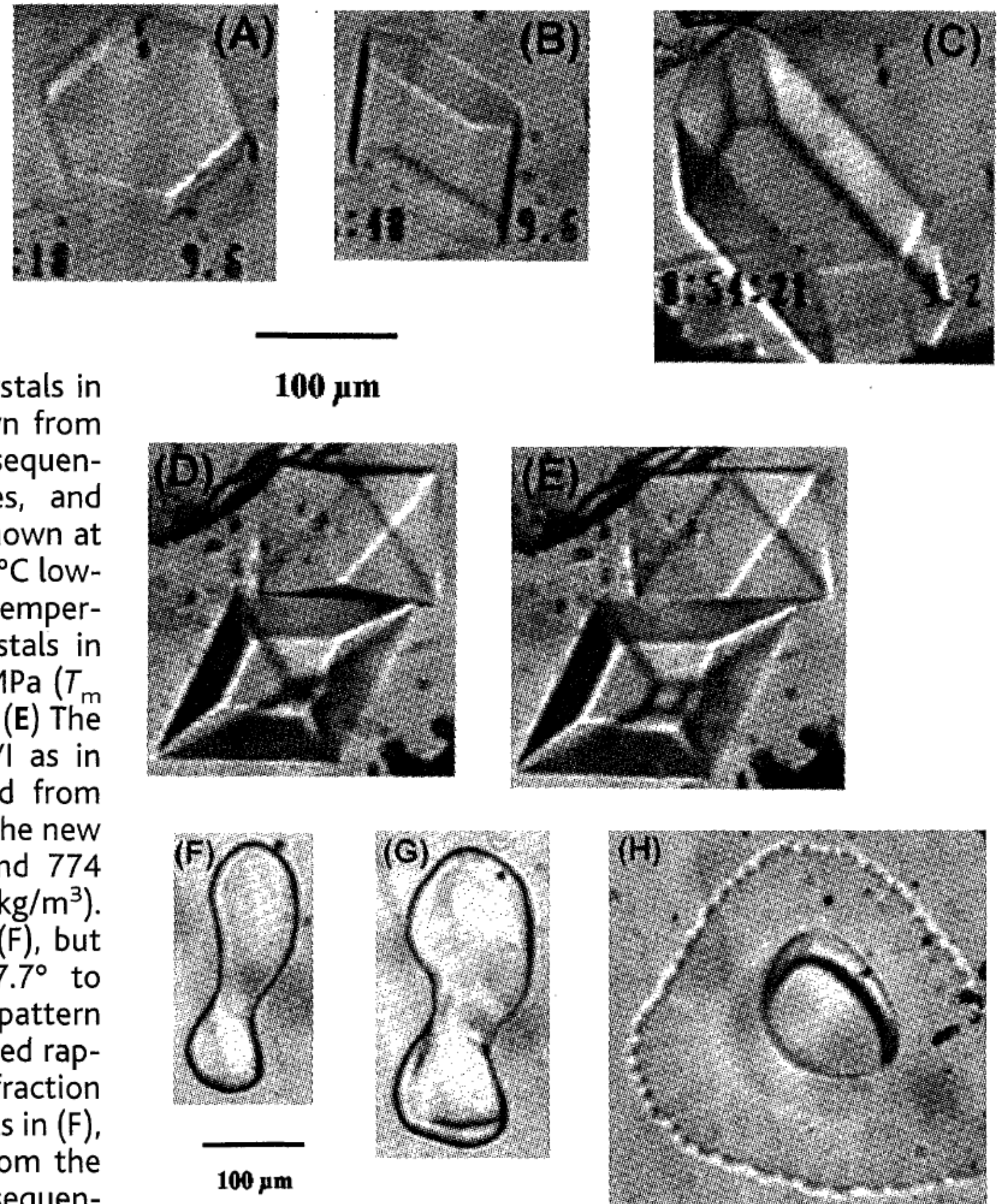

Fig. 2. Morphologies and growth patterns of ice V (panels A, B, and C), ice VI (panels D and E), and the new phase (panels F, G, and H). (**A** and **B**) Ice V in water at 9.8°C and 855 MPa (T_m = 10.1°C; density ρ = 1226 kg/m^3). (**C**) Ice V in water at 9.4°C and 845 MPa. The ice V crystals in (A), (B), and (C) were grown from the same crystallite seed in sequential warming-cooling cycles, and the temperature readings shown at lower right corners were 0.2°C lower than the respective true temperatures. (**D**) Two ice VI crystals in water at 40.9°C and 1241 MPa (T_m = 42.6°C; ρ = 1268 kg/m^3). (**E**) The same two crystals of ice VI as in (D), but which were cooled from 40.9° to 40.3°C in 29 s. (**F**) The new phase in water at 7.7°C and 774 MPa (T_m = 8.1°C; ρ = 1212 kg/m^3). (**G**) The same crystal as in (F), but which was cooled from 7.7° to 7.0°C in 9 s. (**H**) The growth pattern of the new phase when cooled rapidly from 7.9° to 7.2°C in a fraction of a second. Note the crystals in (F), (G), and (H) were grown from the same crystallite nucleus in sequential warming-cooling cycles.

Fig. 4. Raman spectra of the new ice phase compared with ices I, II, III, V, VI, and water measured in situ in the diamond cell. Ice I is proton disordered; ice II is proton ordered; ice III is partially proton disordered but has a proton-ordered form (ice IX); ice V is partially proton disordered. We suggest that ice VI is partially ordered as well. The spectrum of supercooled water is in good agreement with previous work [for example (27)]. Weak peaks <100 cm^{-1} in that spectrum arise from spurious scattering. The tick marks denote characteristic Raman peaks discussed in the text: bands at 192, 490, 3215, and 3410 cm^{-1} for the new phase; 145 and 157 cm^{-1} for ice VI; and 95 and 190 cm^{-1} for ice III. Intensity is given in arbitrary units. Detailed analysis of the spectra of the additional phases will be presented elsewhere.

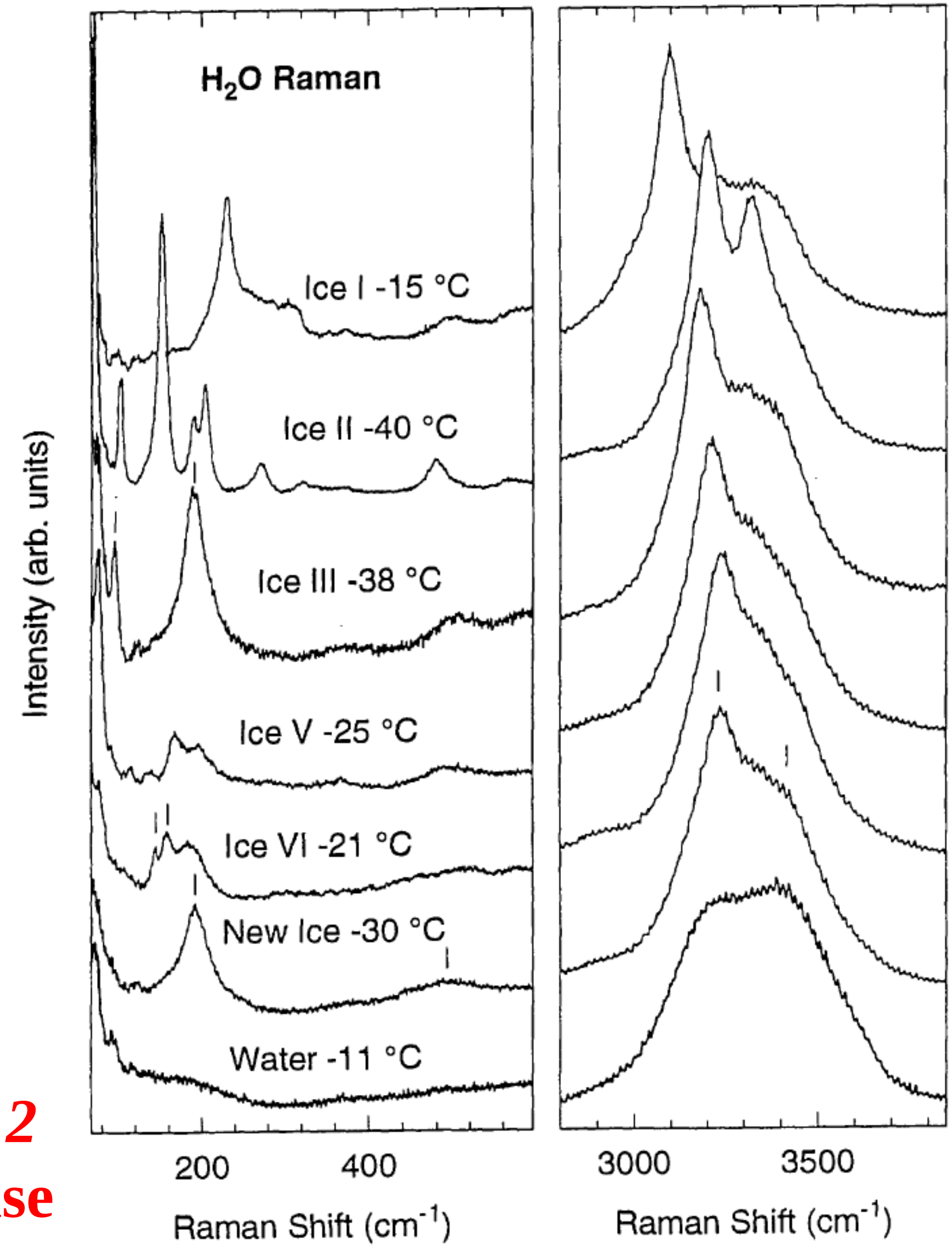

Chou et al. (1998)

Science, v. 281, 809-812

A new liquidus ice phase

HDAC system at USGS

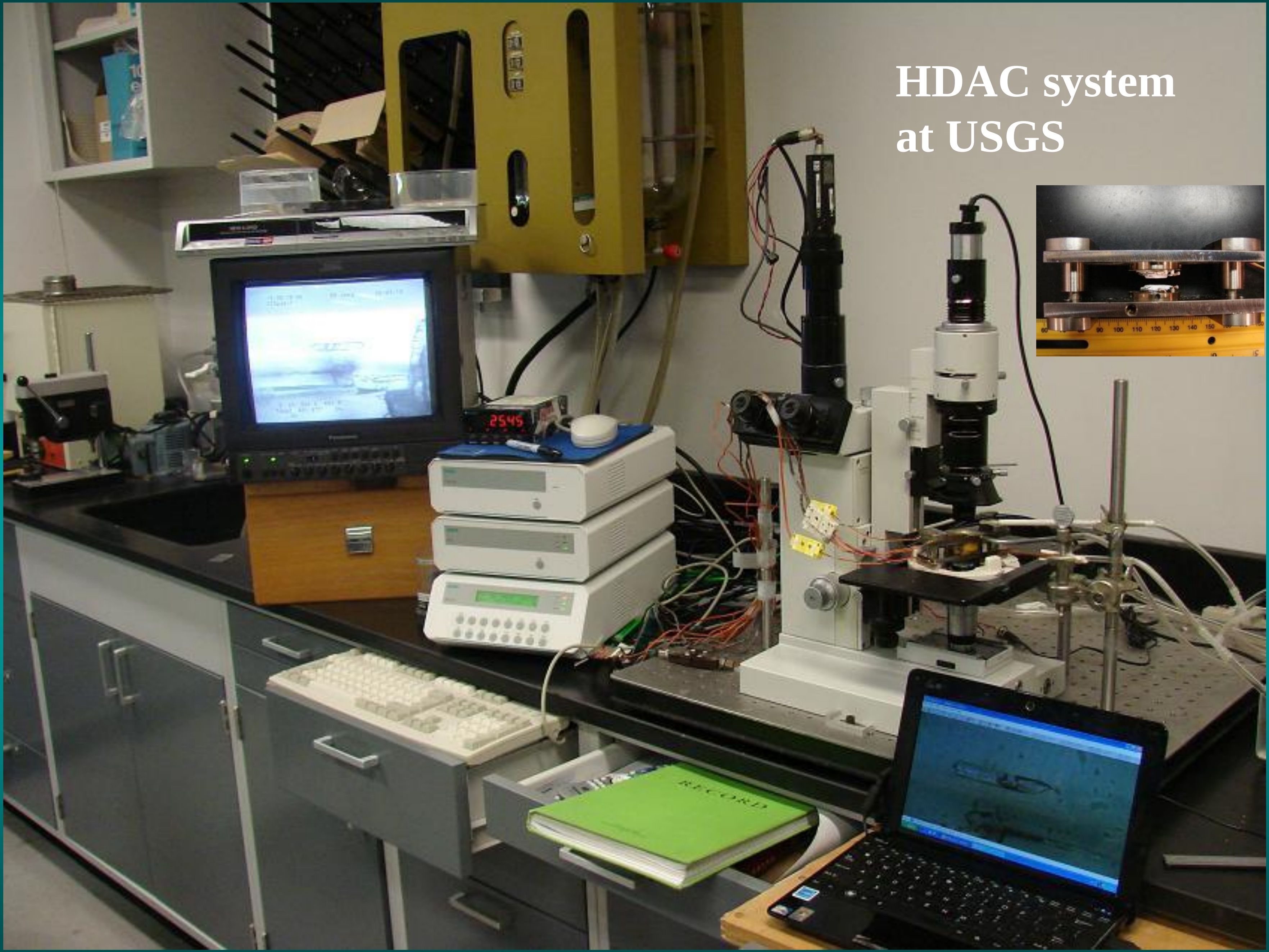

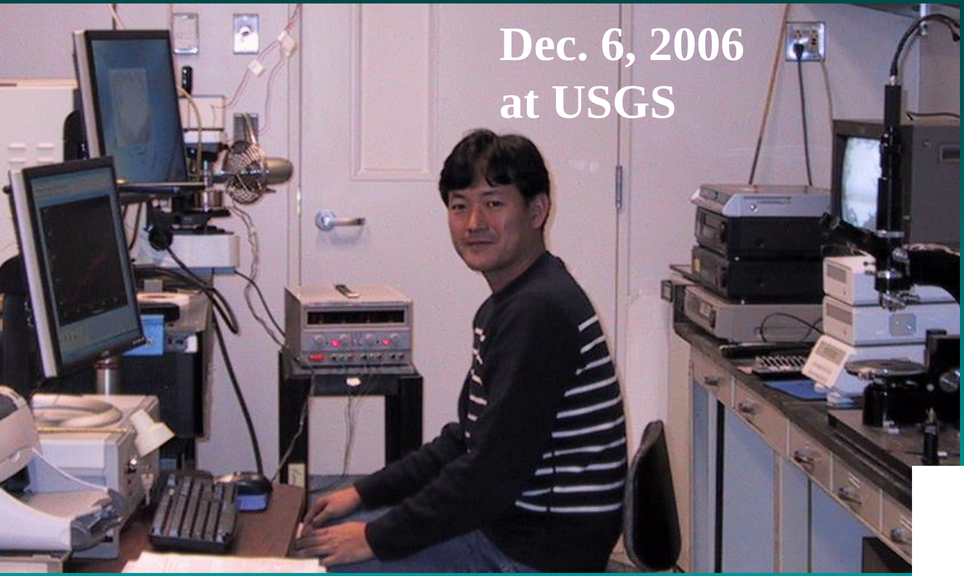

Raman study of synthetic subduction-zone fluids ($KAlSi_3O_8$-H_2O) system

Mibe, Chou, & Bassett
JGR, 113 (2008)

Kenji Mibe
Earthquake Research Institute
University of Tokyo, Japan

SCF: supercritical fluid
F: aqueous fluid
Sa: sanidine
M: hydrous melt
Ms: muscovite
C: corundum

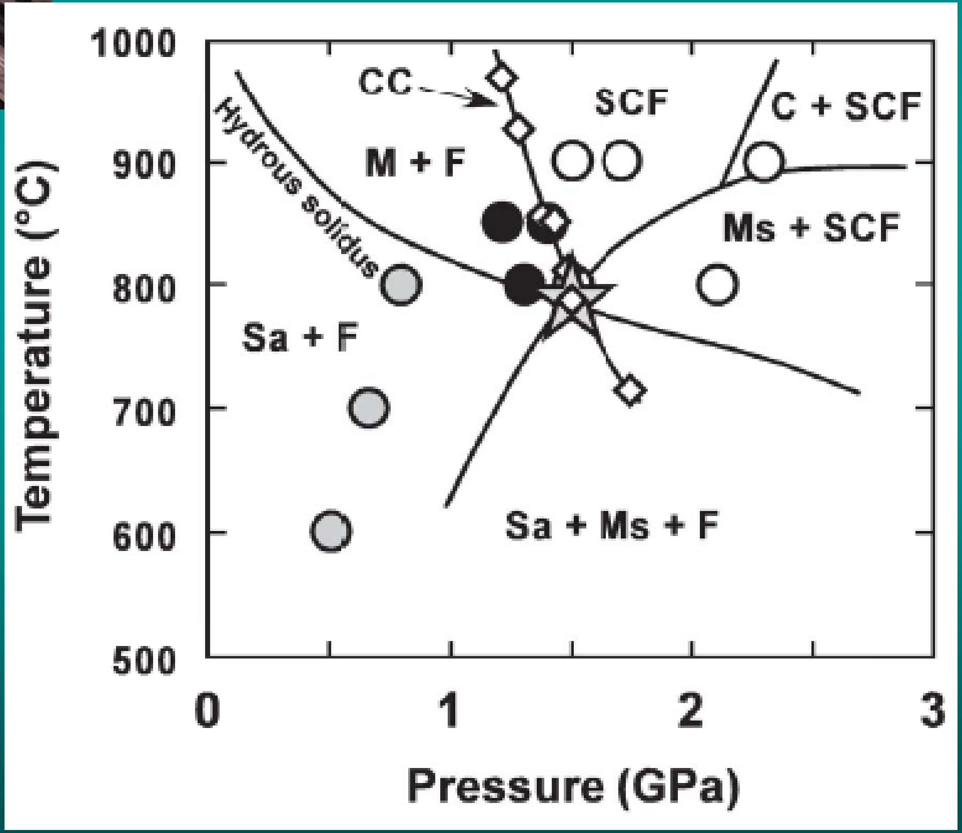

Sanidine
$KAlSi_3O_8$

Muscovite
$KAl_2(Si_3Al)O_{10}(OH)_2$

Some minerals in the system:

$KAlSi_3O_8$ - H_2O

Corundum
Al_2O_3

Mibe, Chou, & Bassett
JGR, 113 (2008)

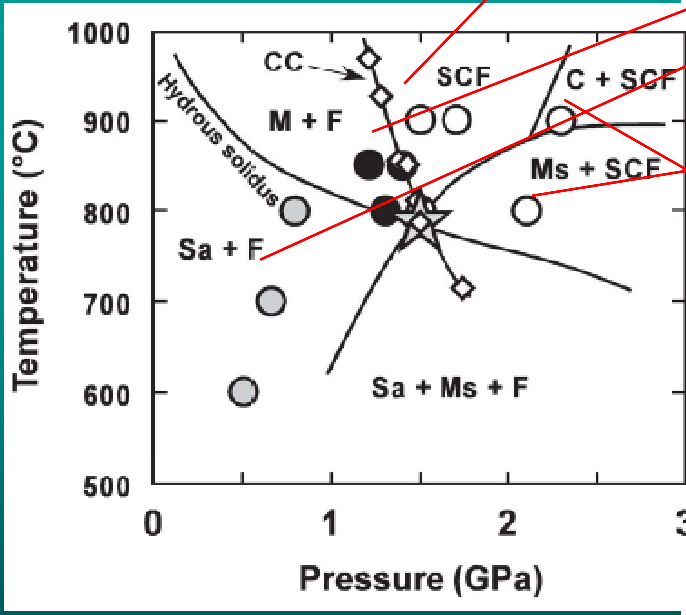

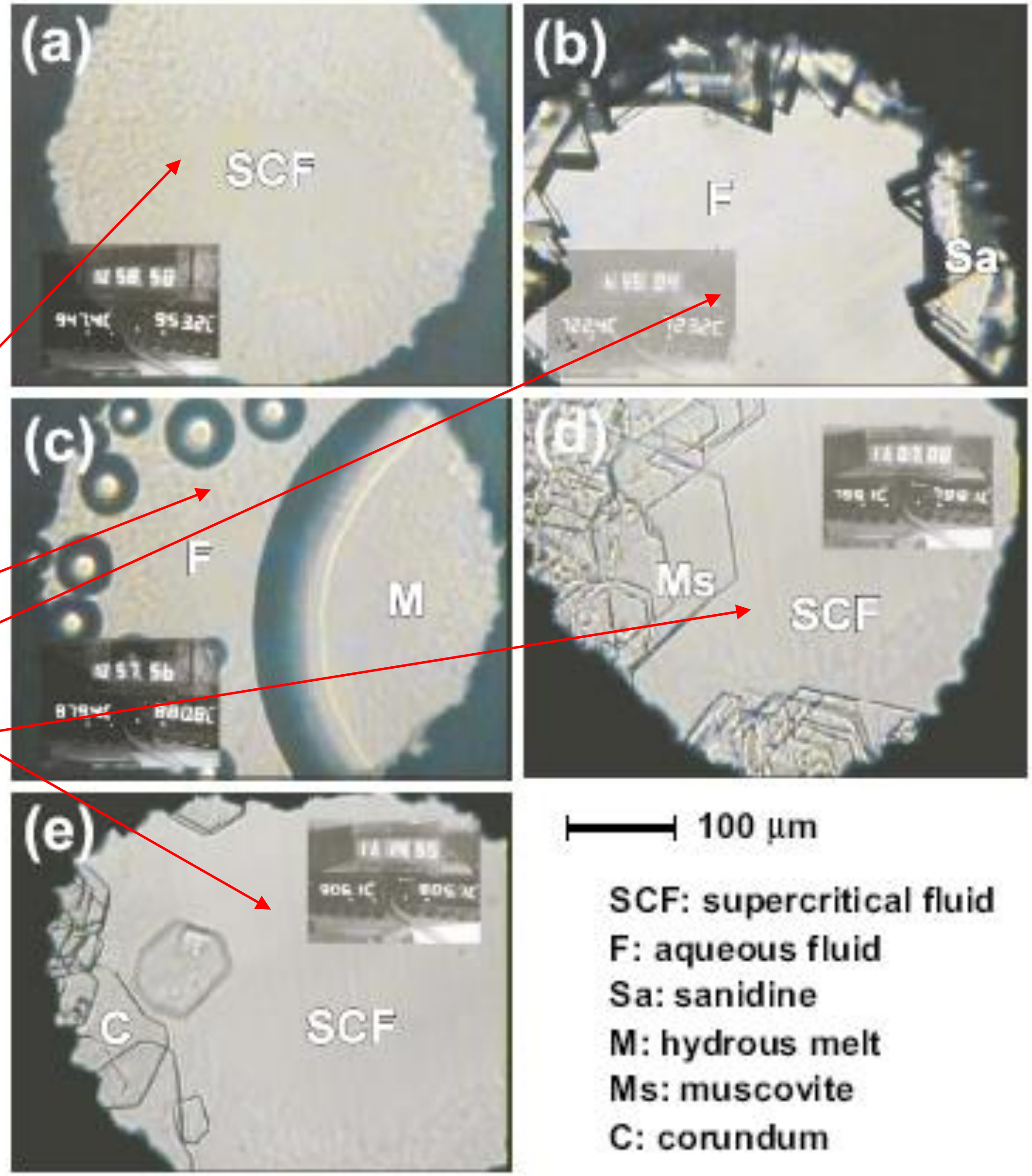

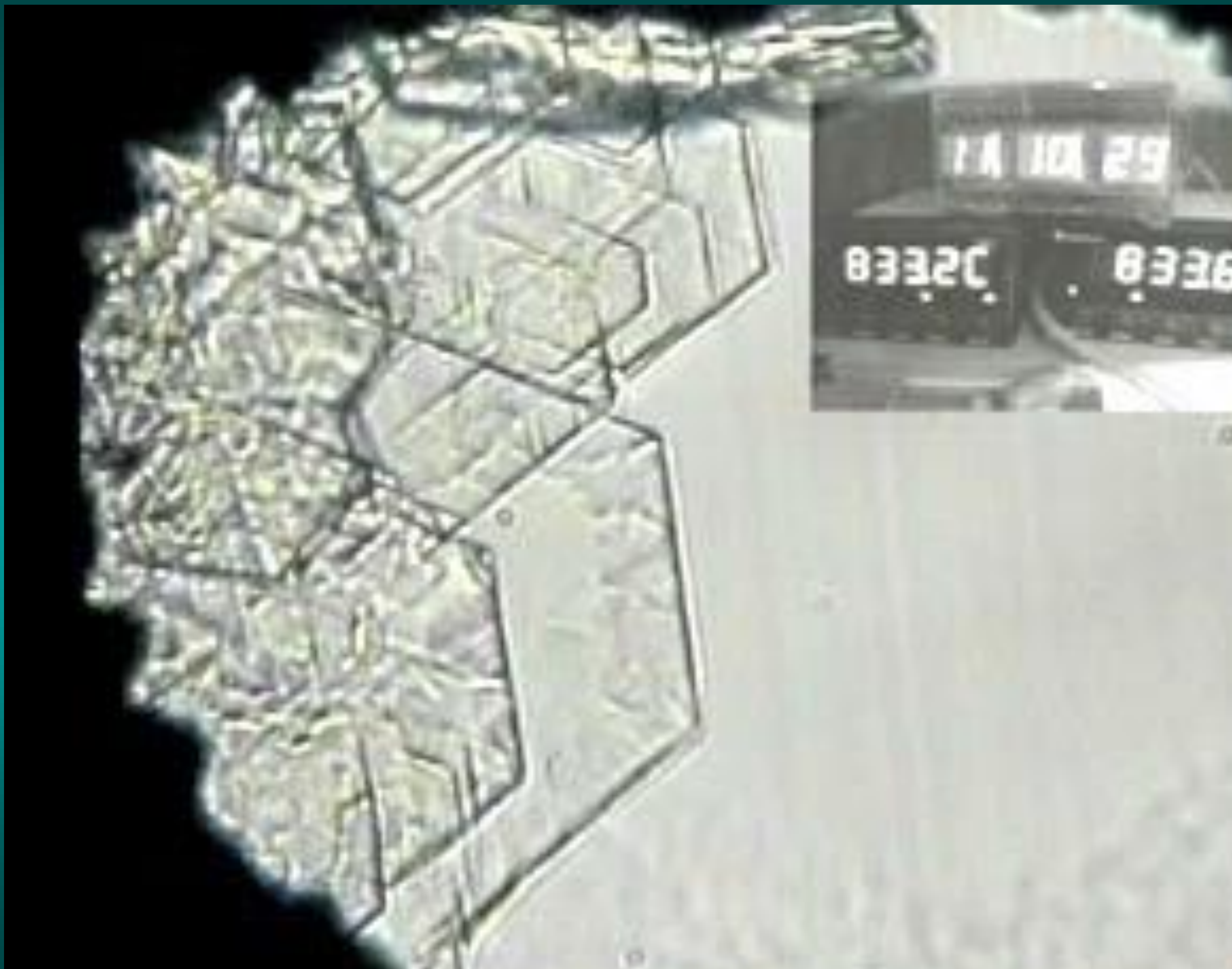


10 58 21
938.2C 941.6C

Mibe, Chou, & Bassett

JGR, 113 (2008)

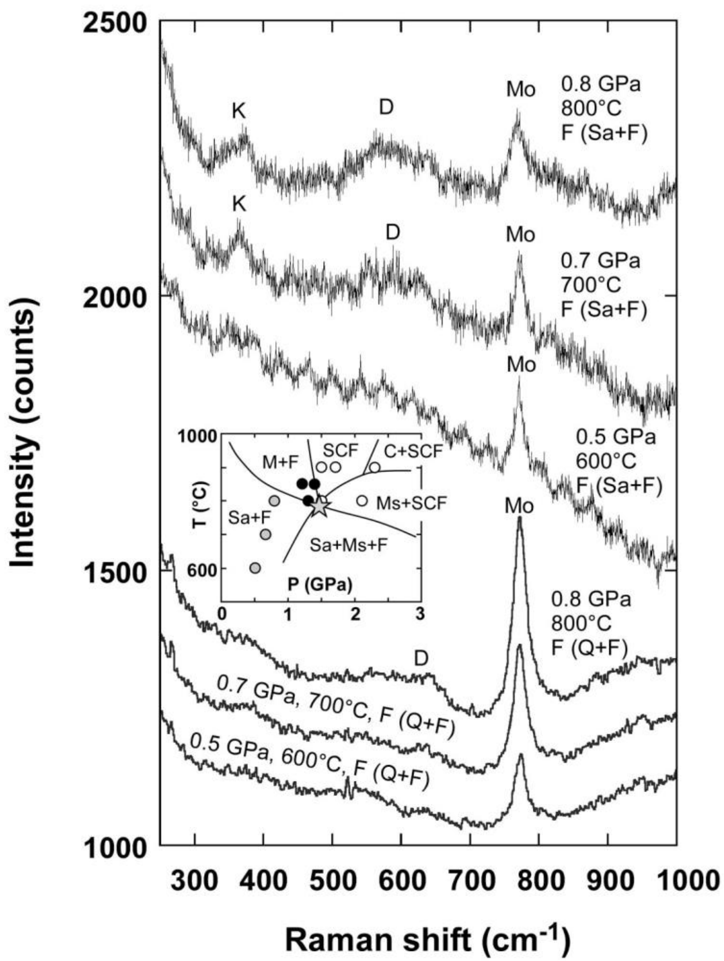

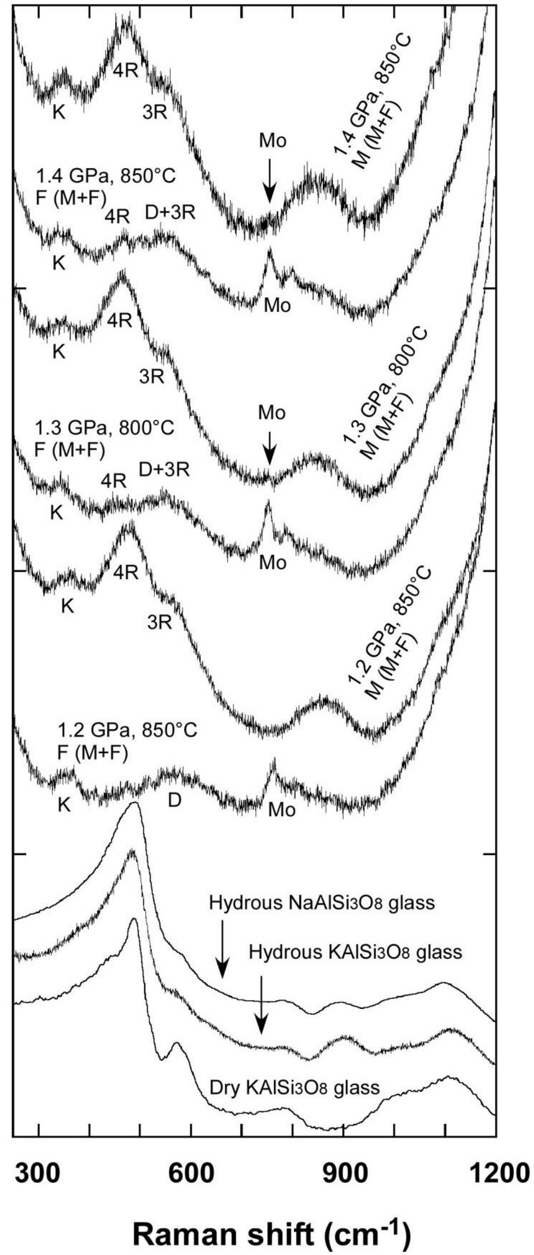

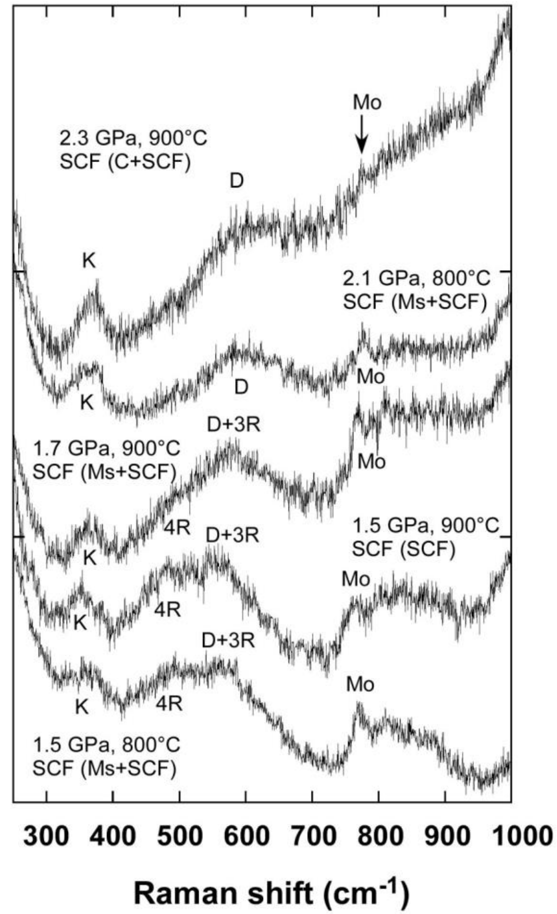

Molecule[a]	Frequency (cm^{-1})[b]	Motion[j]
H_4SiO_4 (Mo)	783 (calc)[c], 785 (exp)[d], 788 (calc)[e]	n(Si-O)
KH_3SiO_4 (Mo)	748 (calc)[f]	n(Si-O)
$H_6Si_2O_7$ (D)	620 (calc)[e], 631 (calc)[c], 638 (calc)[g]	n(Si-O), d(Si-O-Si)
$H_6SiAlO_7^{1-}$ (D)	585 (calc)[g]	n(T[k]-O), d(Si-O-Al)
$H_4SiAlO_7^{3-}$ (D)	574 (exp)[d]	n(T-O), d(Si-O-Al)
$H_6Si_3O_9$ (3R)	629 (calc)[e]	n(Si-O-Si)
$H_6Si_2AlO_9^{1-}$ (3R)	574 (calc)[h]	n(T-O-T)
$H_8Si_4O_{12}$ (4R)	490 (calc)[h]	n(Si-O-Si)
$H_8Si_3AlO_{12}^{1-}$ (4R)	488 (calc)[h]	n(T-O-T)
$Al(OH)_4^{1-}$	616 (calc)[i], 620 (exp)[d]	n(Al-O)
$KAl(OH)_4$	619 (calc)[f]	n(Al-O)
KH_2AlO_3	691 (calc)[f]	n(Al-O)
$Al(OH)_3H_2O$	438 (calc)[i]	n(Al-OH_2)
KOH	361 (calc)[f]	d(K-O-H)

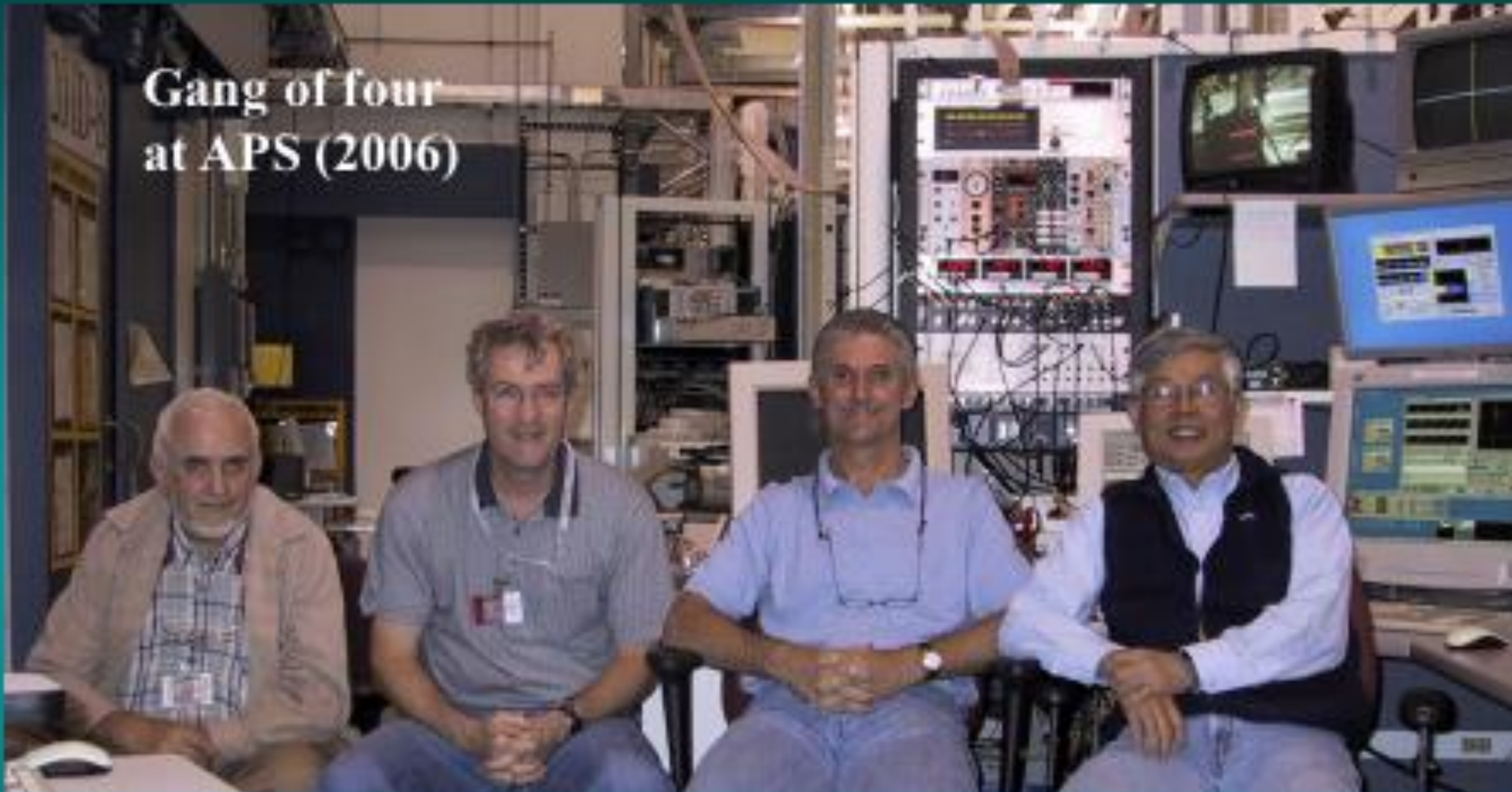

William
Bassett
Cornell Univ.
USA

Alan
Anderson
St. Francis
Xavier Univ.
Canada

Robert
Mayanovic
Missouri State Univ.
USA

I-Ming
Chou
USGS

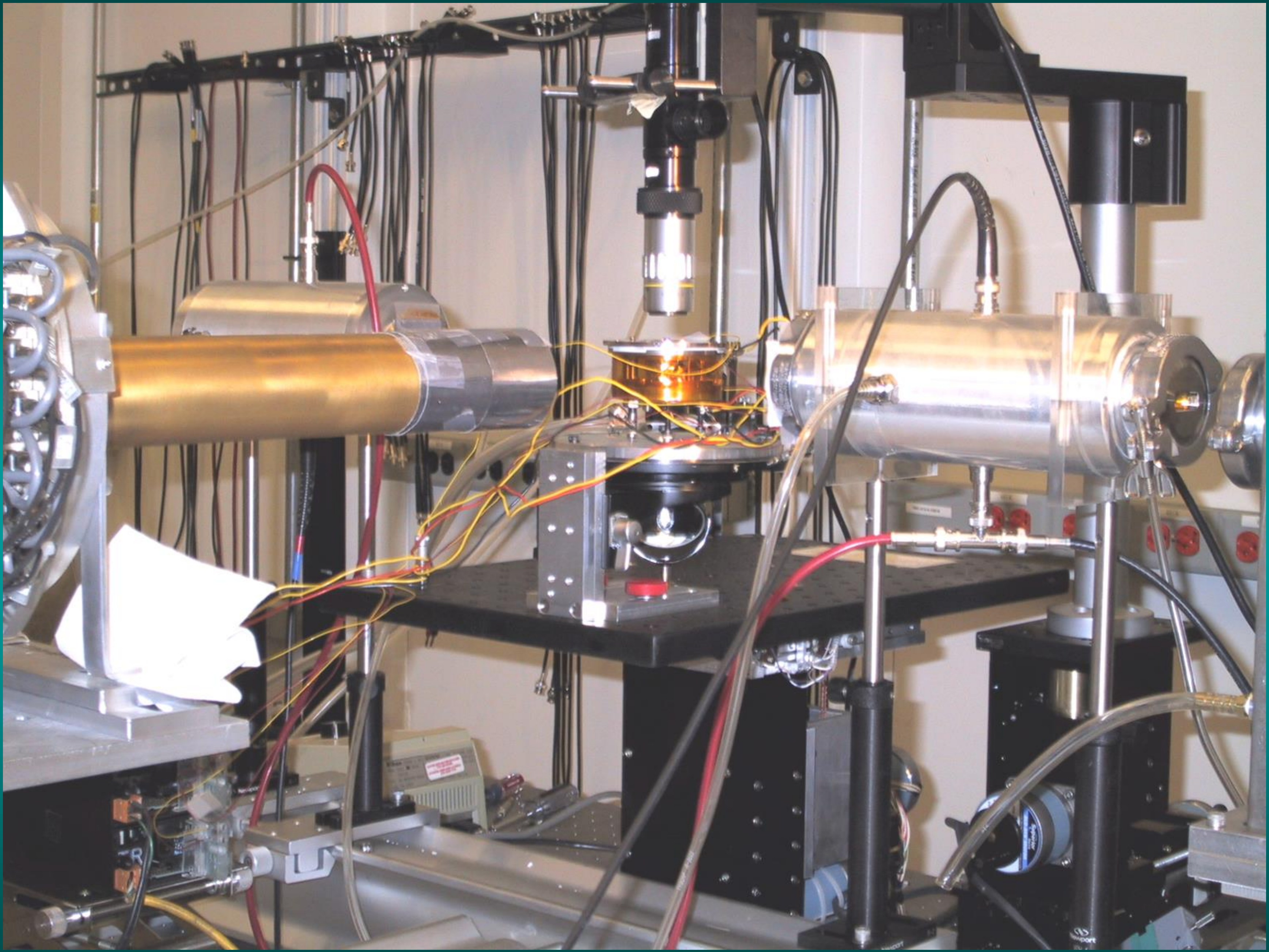

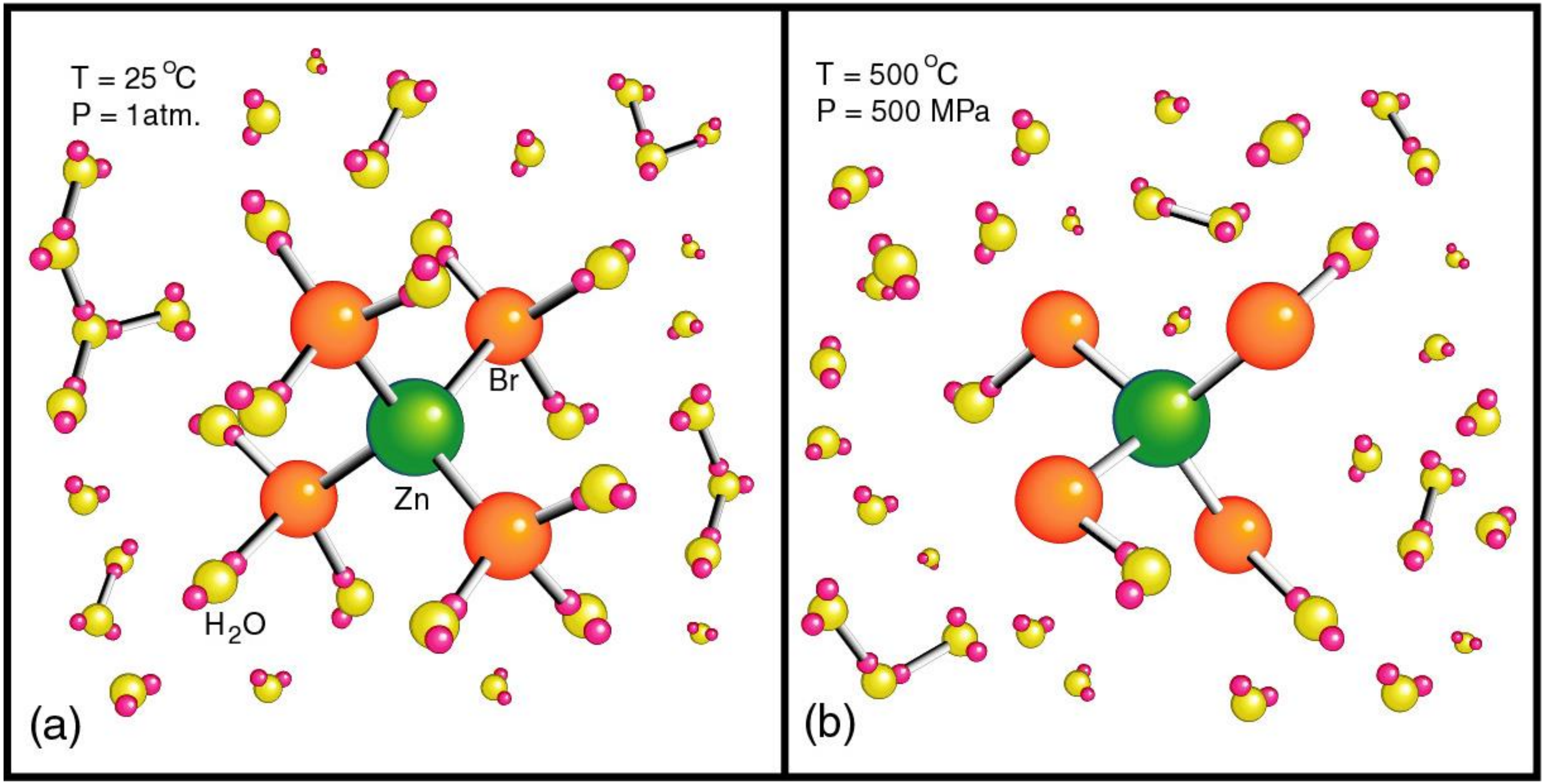

in 1*m* $ZnBr_2$/6*m* NaBr solution, $ZnBr_4^{2-}$ predominant

Zn-Br bond length - 0.005 Å/100 ˚C

XAS: X-ray Absorption Spectroscopy

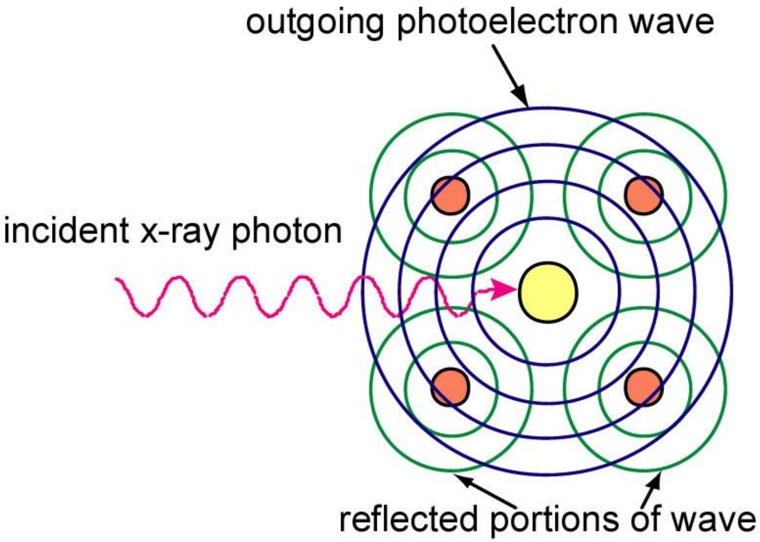

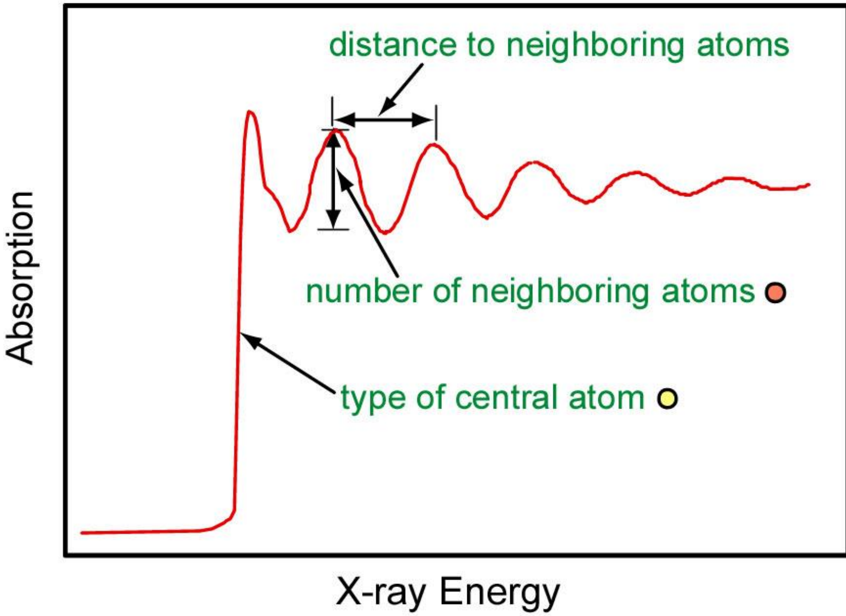

Hydrothermal Diamond Anvil Cell

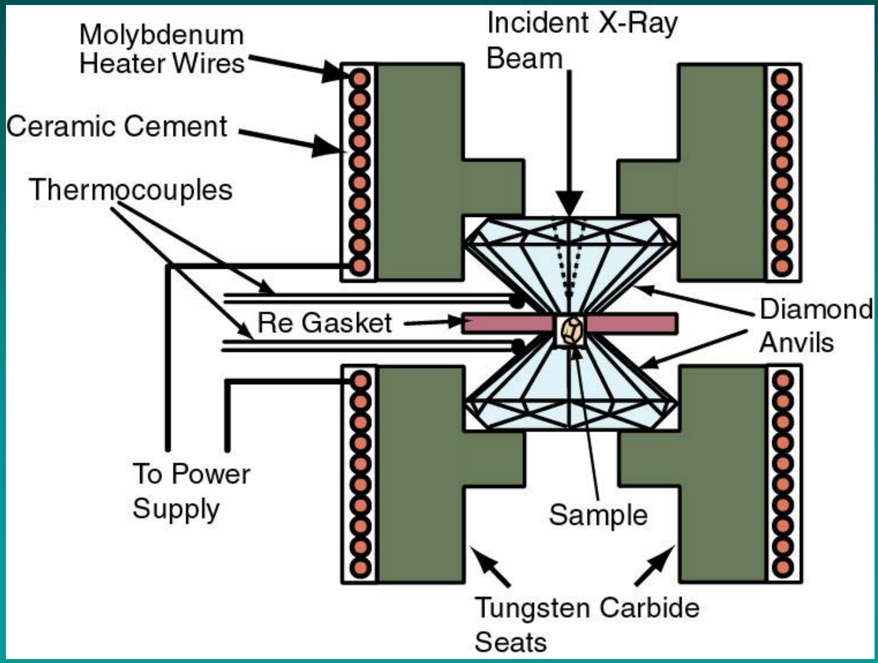

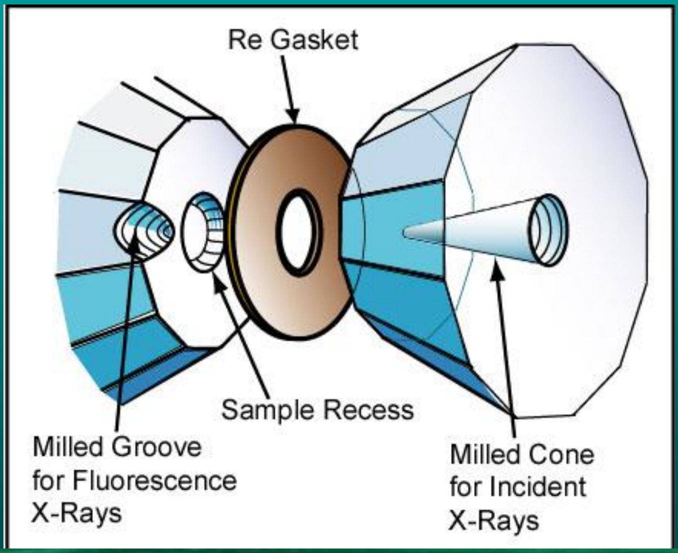

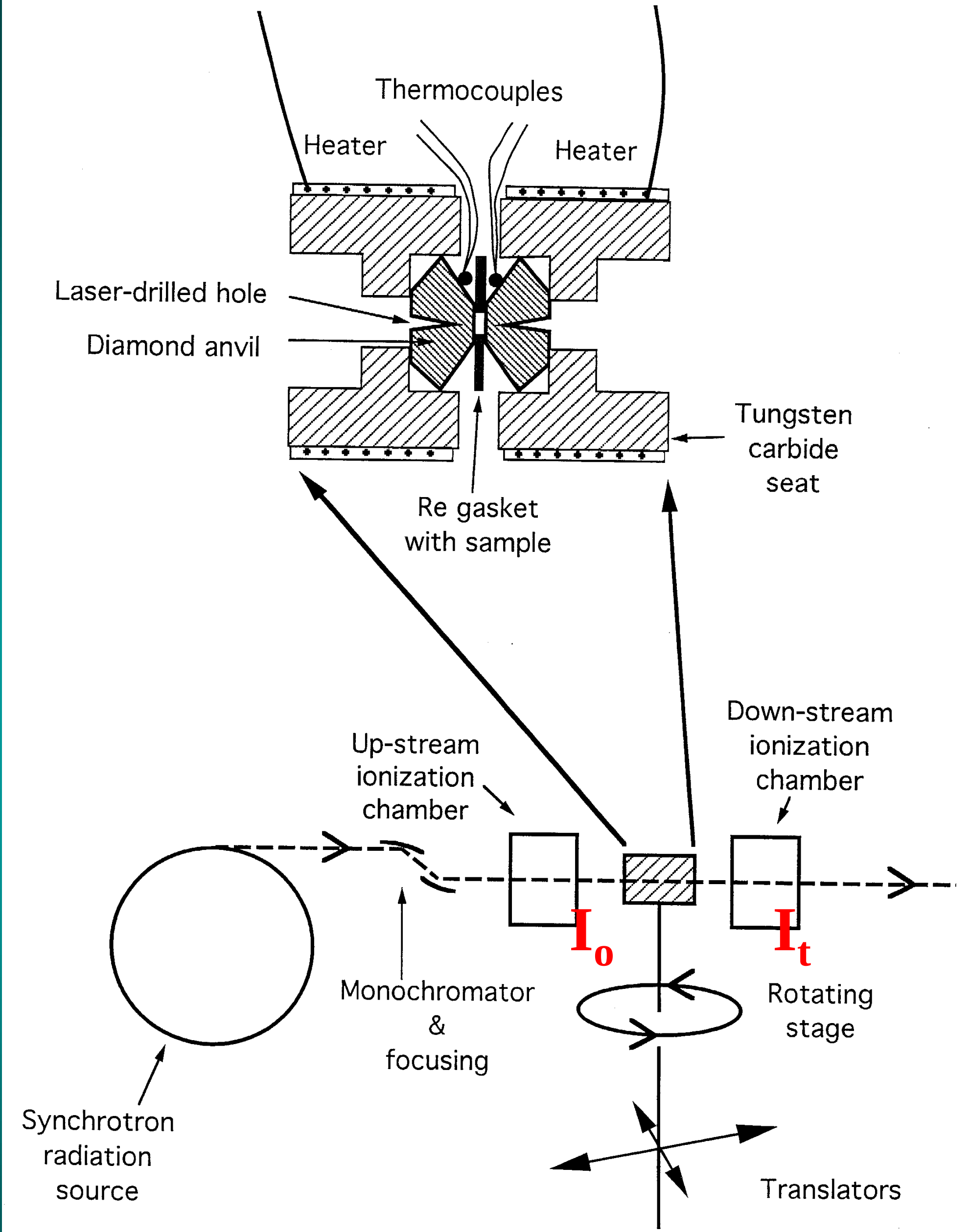

Thermocouples
Heater
Heater
Laser-drilled hole
Diamond anvil
Tungsten carbide seat
Re gasket with sample
Up-stream ionization chamber
Down-stream ionization chamber
I_o
I_t
Monochromator & focusing
Rotating stage
Synchrotron radiation source
Translators

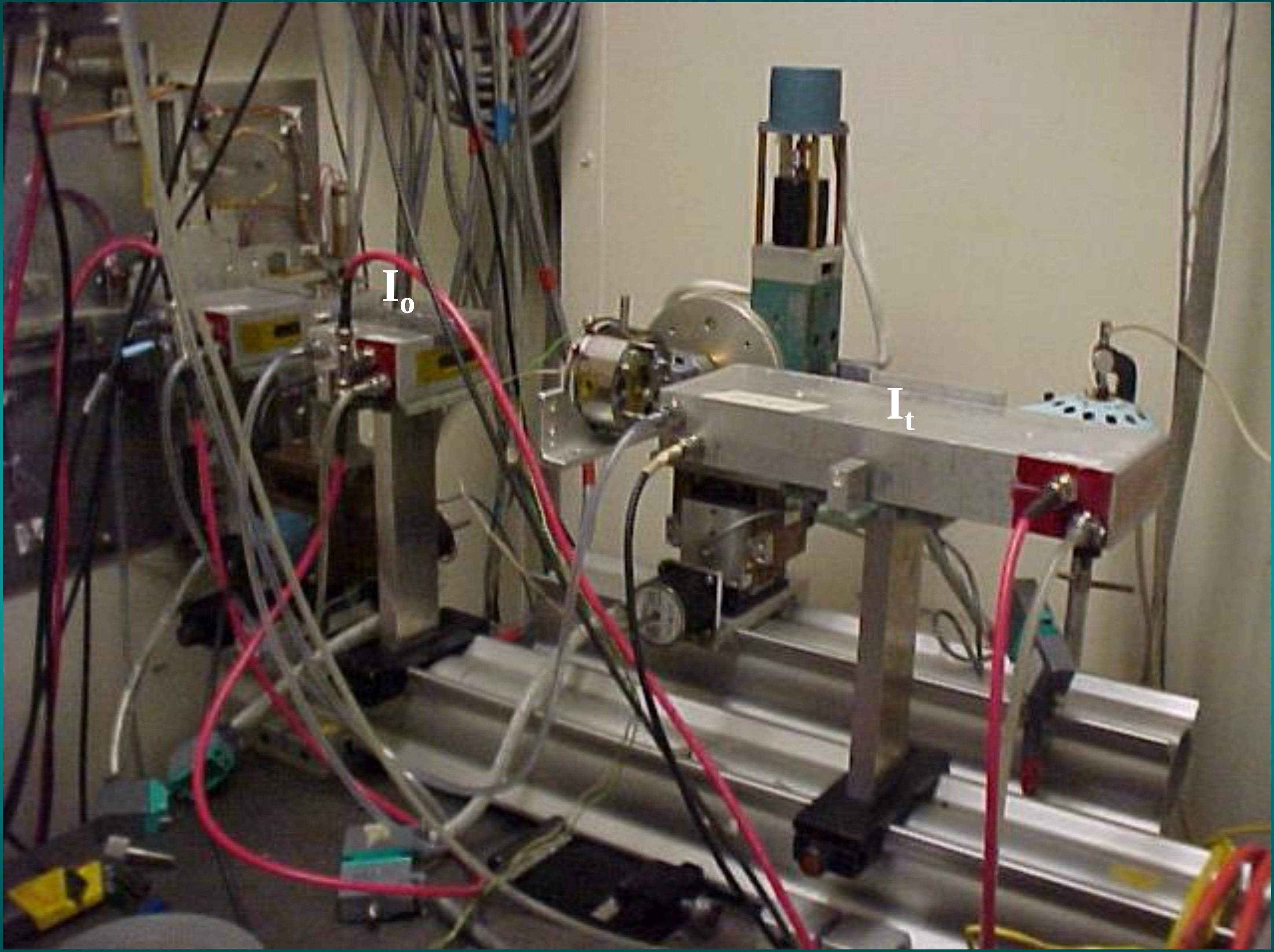
I_o
I_t

CHESS
5.29 GeV
220 mA max.

ln (I_o/I_t)

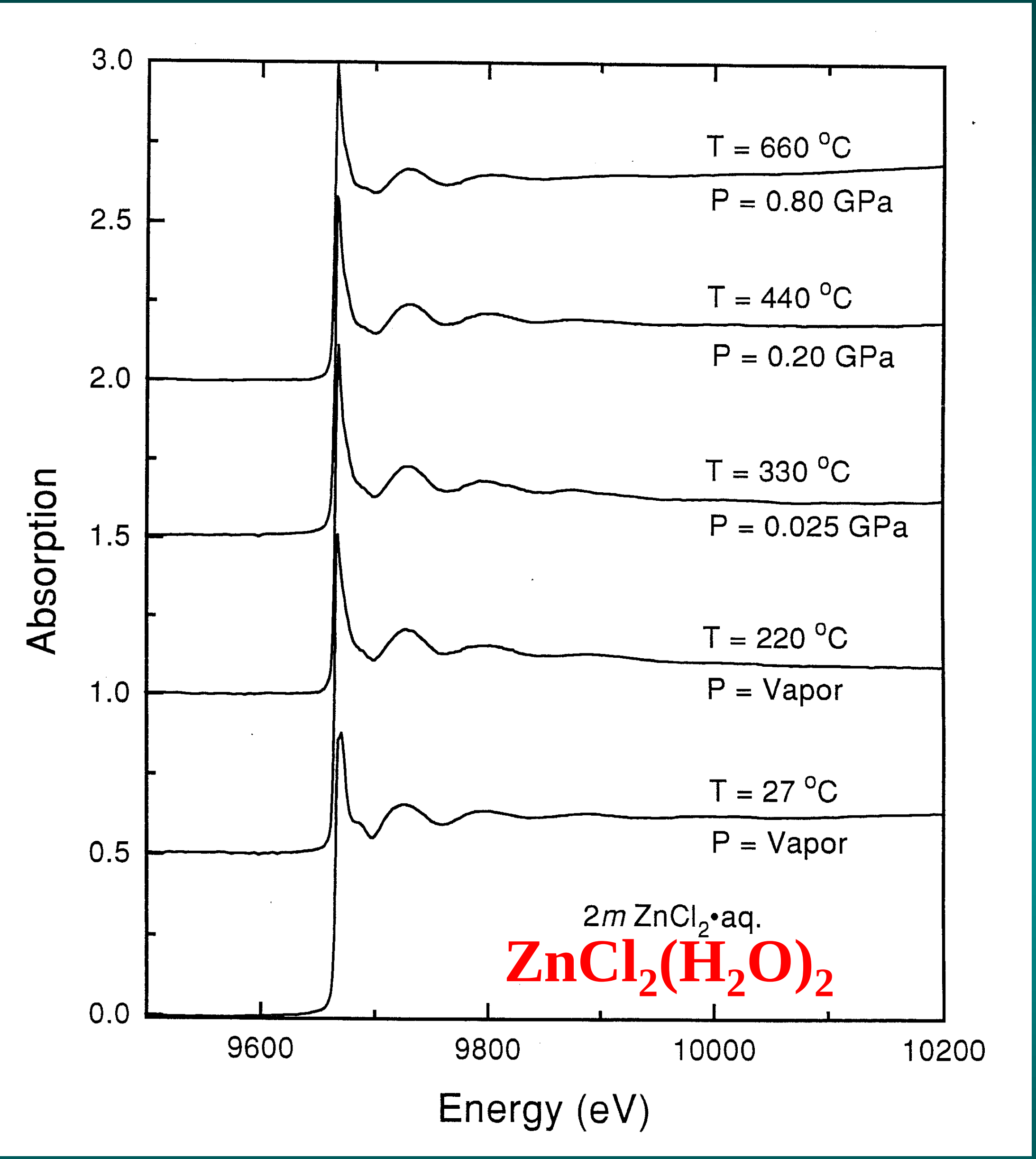

in 1*m* $ZnCl_2$/6*m* NaCl solution:
$ZnCl_4^{2-}$ predominant

anti-Stokes

Mibe & G-4
1*m* $ZnBr_2$/6*m* NaBr
Br / Zn = 8

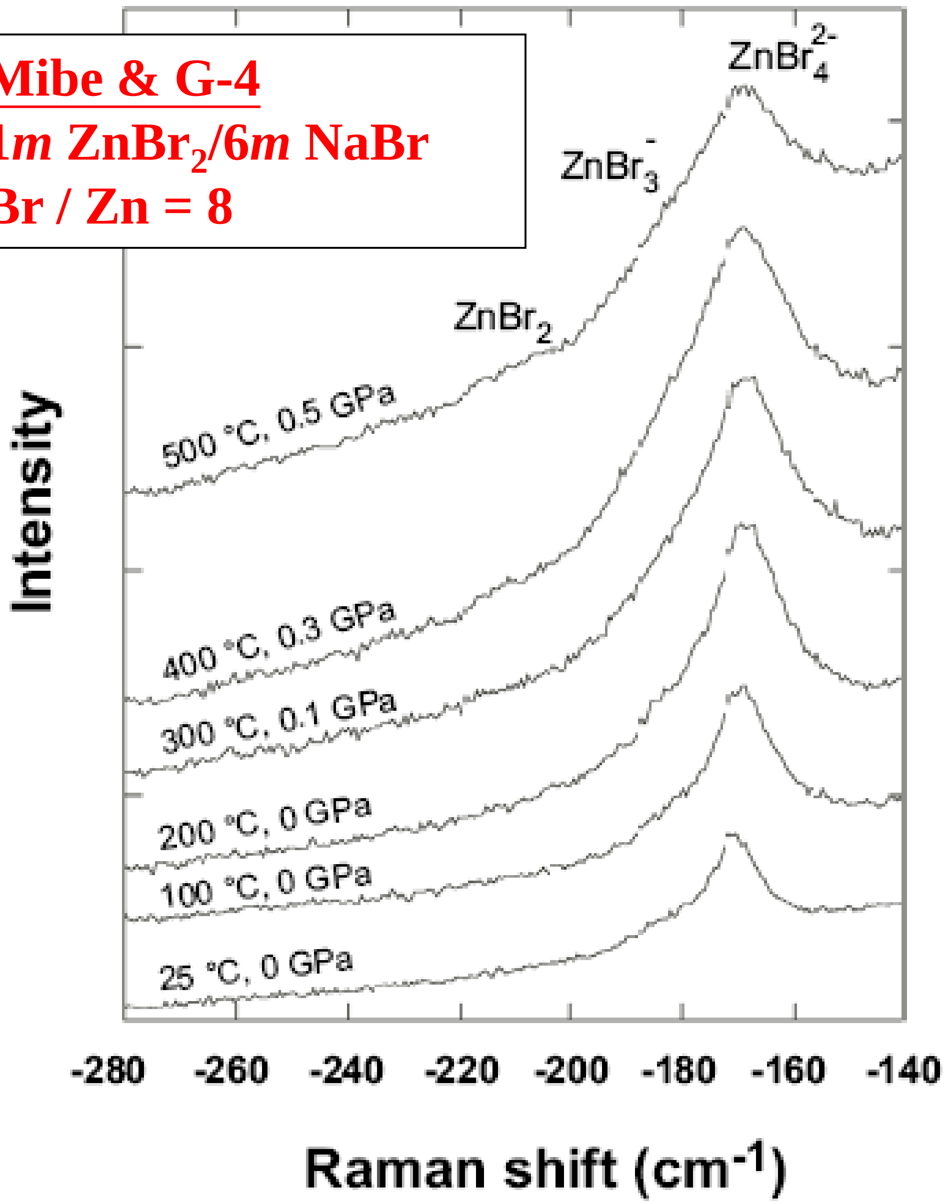

Stokes

Yang, Crerar, & Irish (1988)
1.8 *m* Zn^{2+}; 5.02 *m* Br^-
(Br / Zn = 2.8)

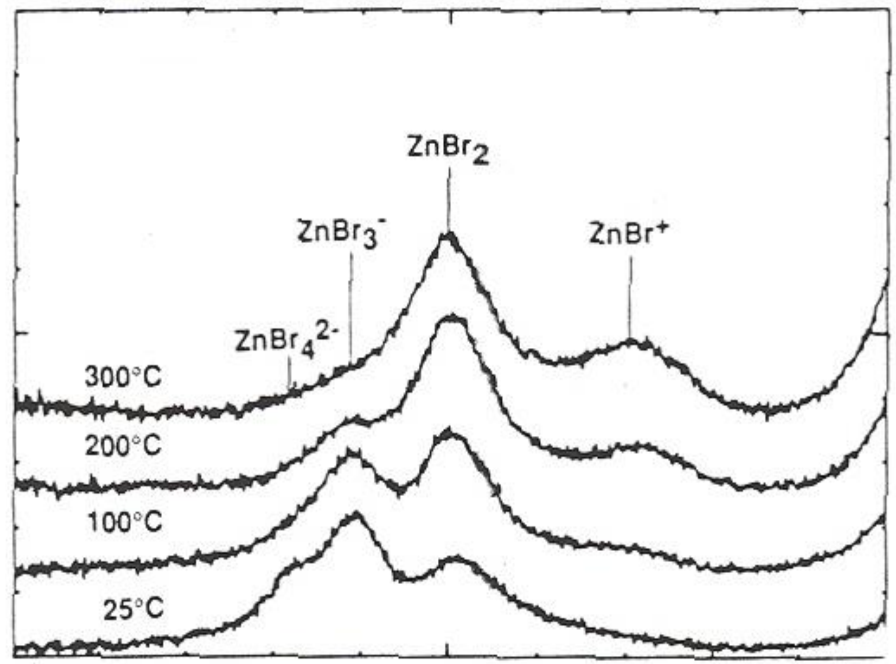

110
205

Raman shift (cm^{-1})

Recent XAFS studies (1998) *Chem. Geol.* –
Y (17.038 keV) Ragnarsdorttir et al.
Cd (26.711 keV) Randall et al.
Sb (30.491 keV) Oelkers et al.
all along L-V curves

Electron binding energy (K 1s)
Mn < Fe < Co < Ni < Cu < Zn

Yb L_3-edge (8.944 keV)
La L_3-edge (5.483 keV)

Anderson et al. (2002)
Amer. Min.

Mn Zn

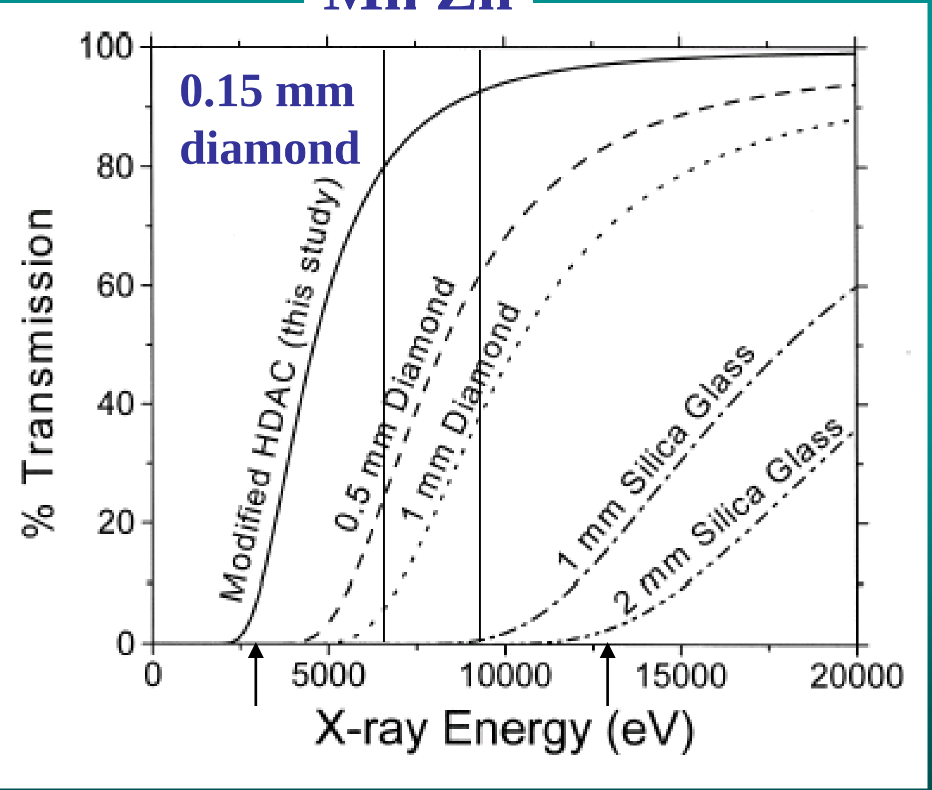

Mayanovic, Anderson, Bassett, & Chou
Rev. Sci. Instrum. 78, 2007;
Amer. Mineral. 94, 2009

Or click on the image.

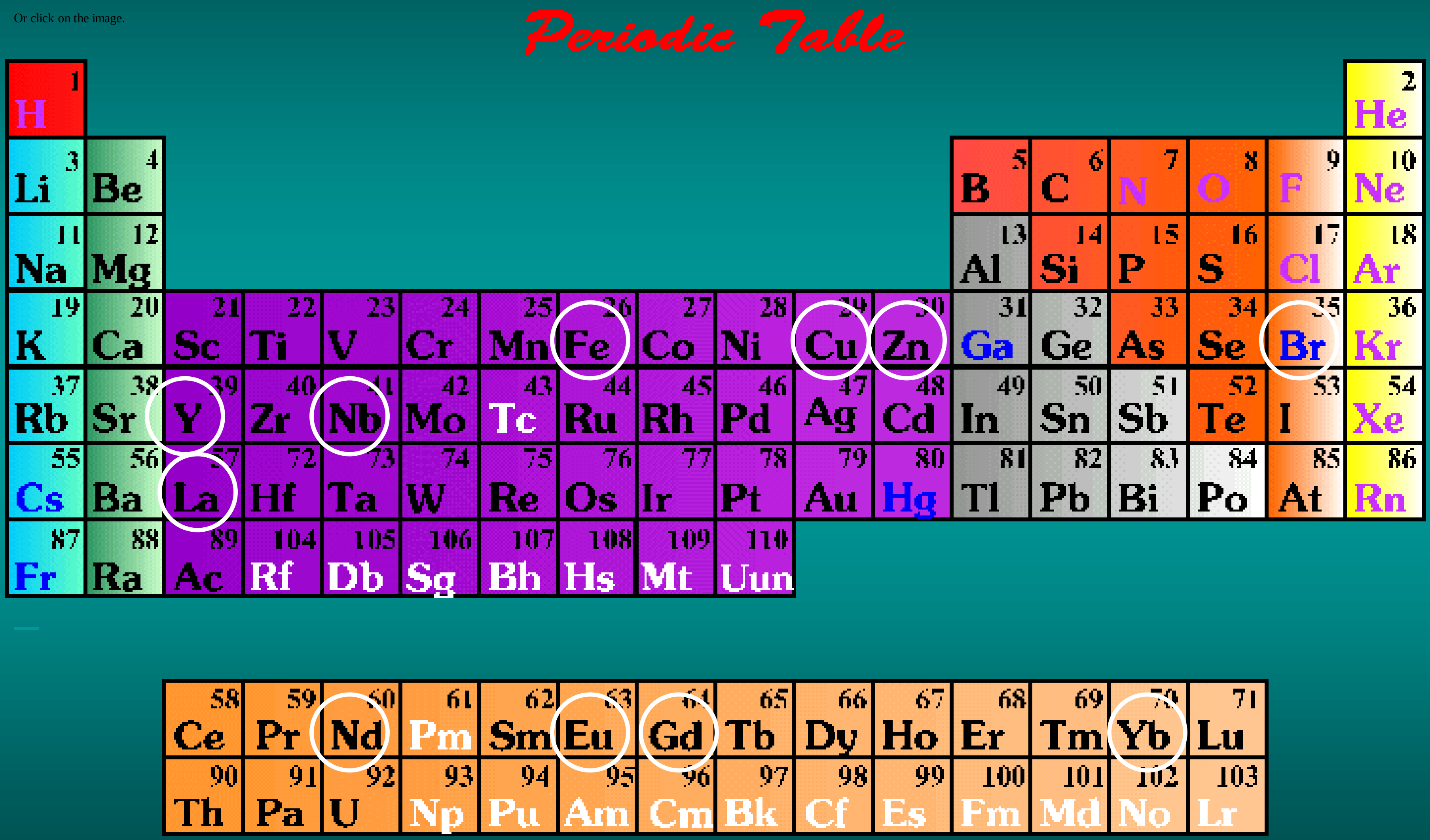

Mayanovic et al. (2002) *J. Phys. Chem.*

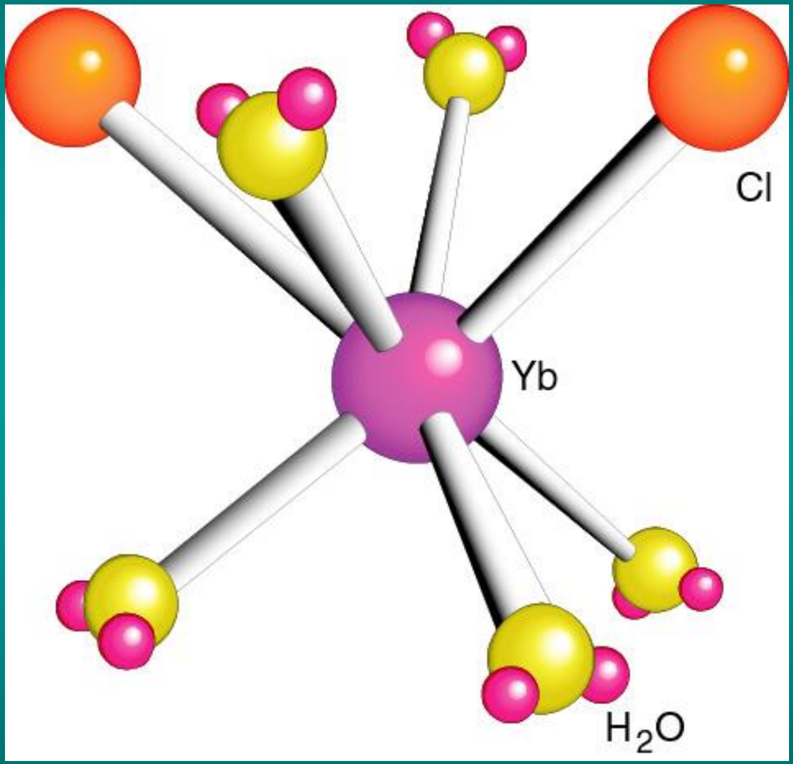

0.006 m $YbCl_3$

0.017 m HCl

$Yb(H_2O)_5Cl_2^+$
Predominant at 500 ˚C

Other aqueous species include stepwise complexes $Yb(H_2O)_{x-n}Cl_n^{+3-n}$
(x = 7; n = 0, 1, 2, and 3), which are stable from
300 to 500 ˚C

**Schmidt et al.
(1998, Am Min.,
v. 83, 995-1007)**

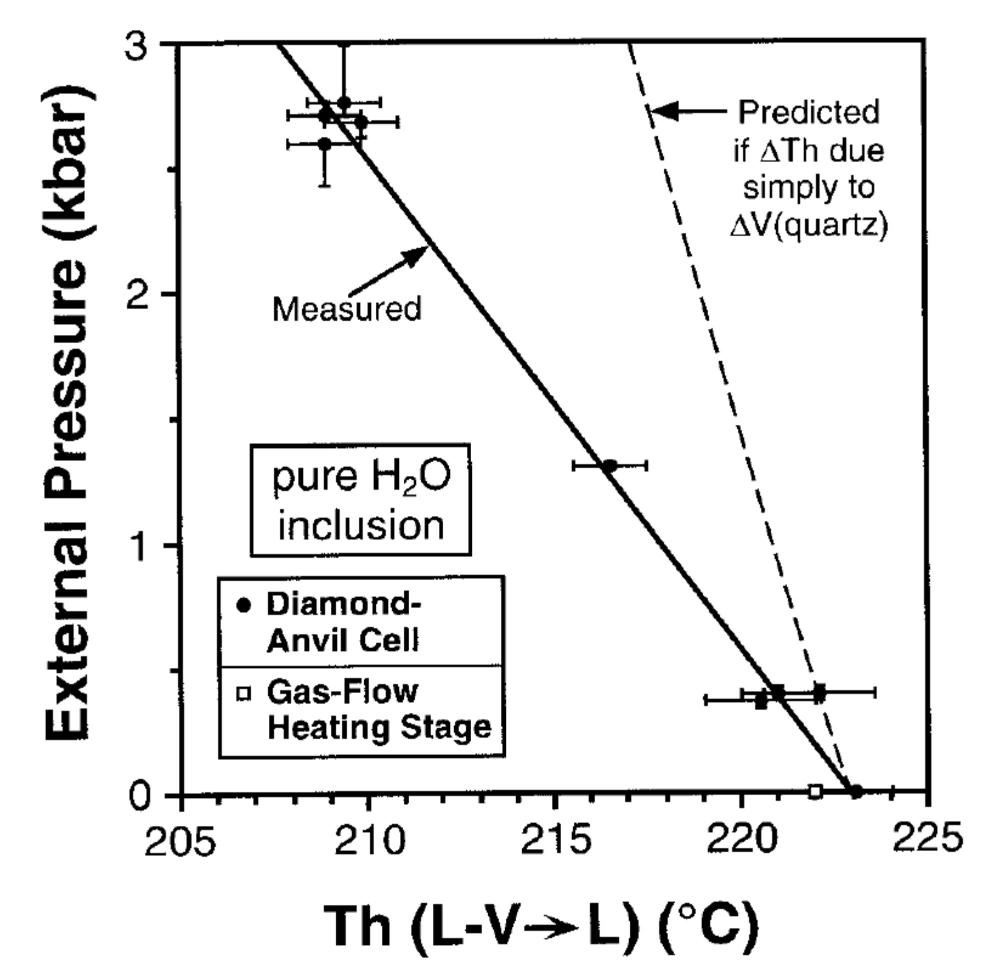

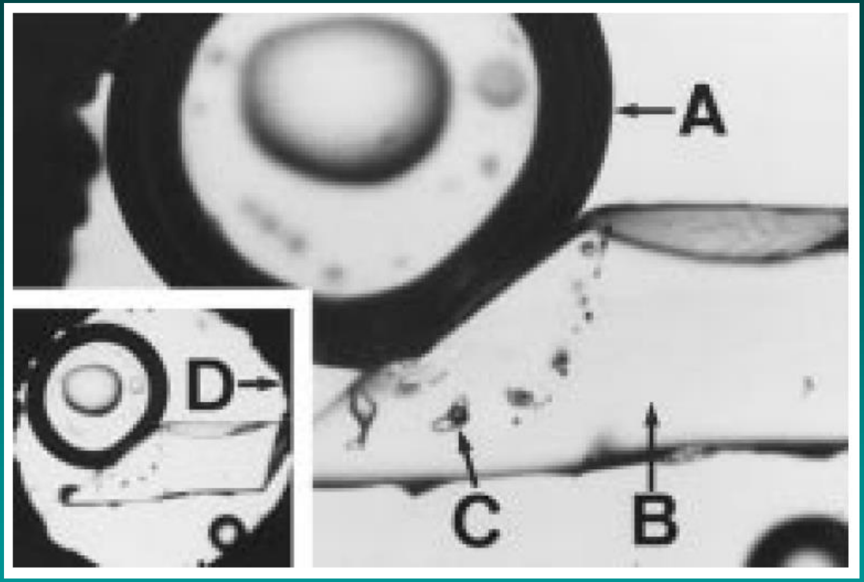

Homogenization T measurements under elevated external P in HDAC for synthetic pure H_2O inclusion in quartz

Summary & Future Works

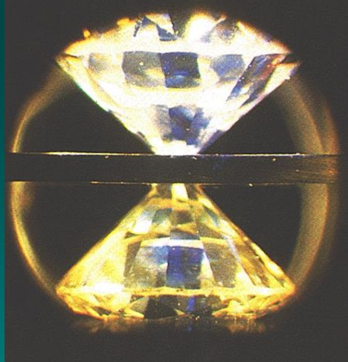

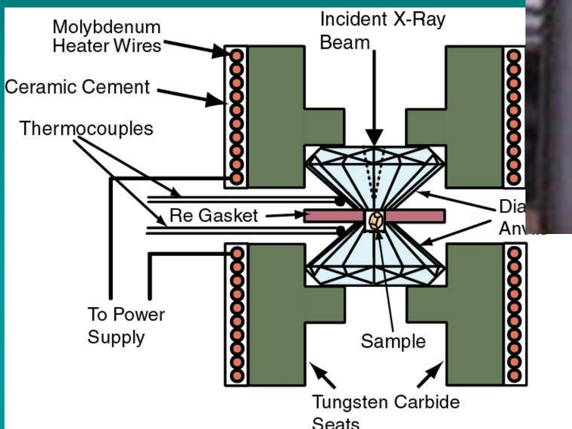

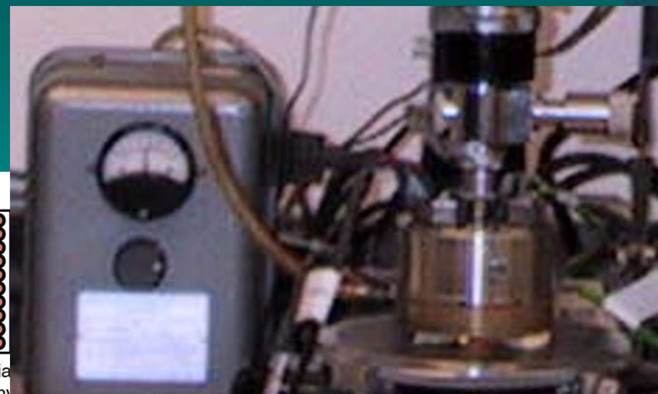

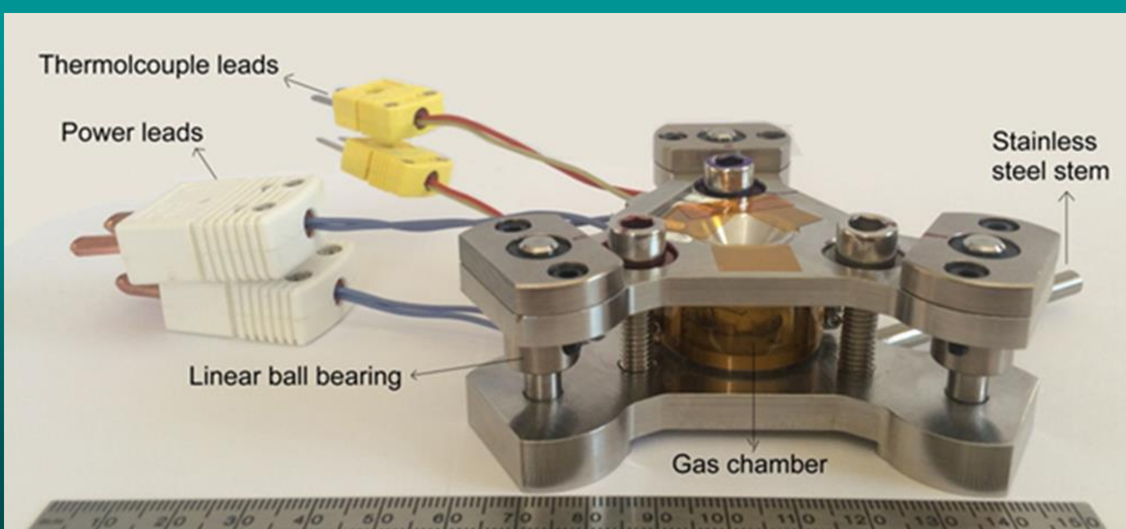

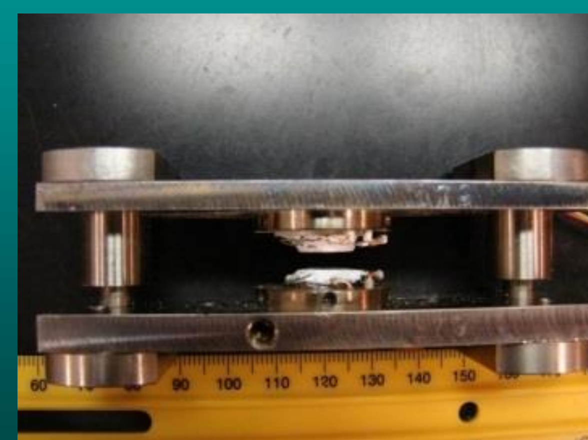

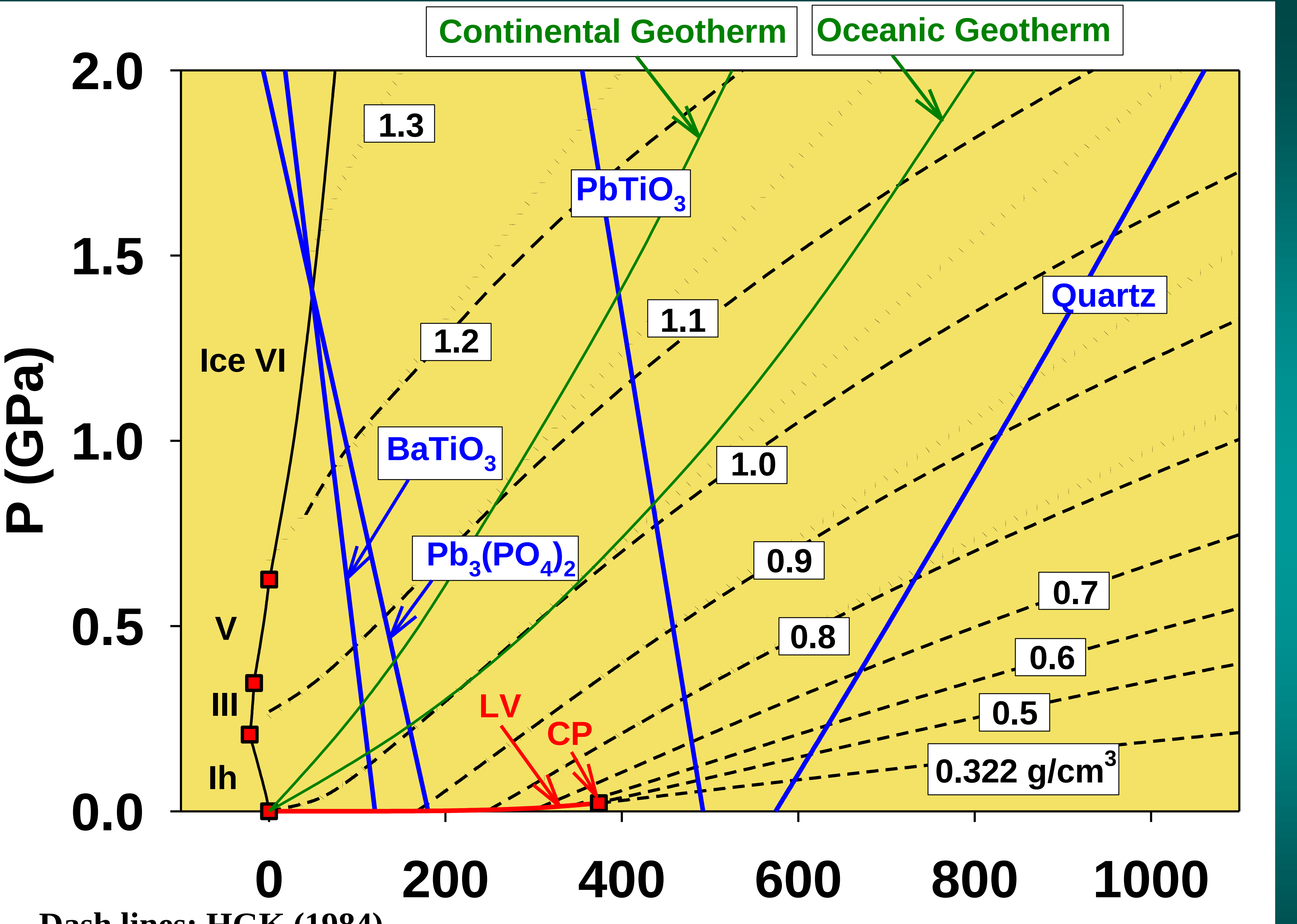

Dash lines: HGK (1984)

Dotted lines: SW (1989)

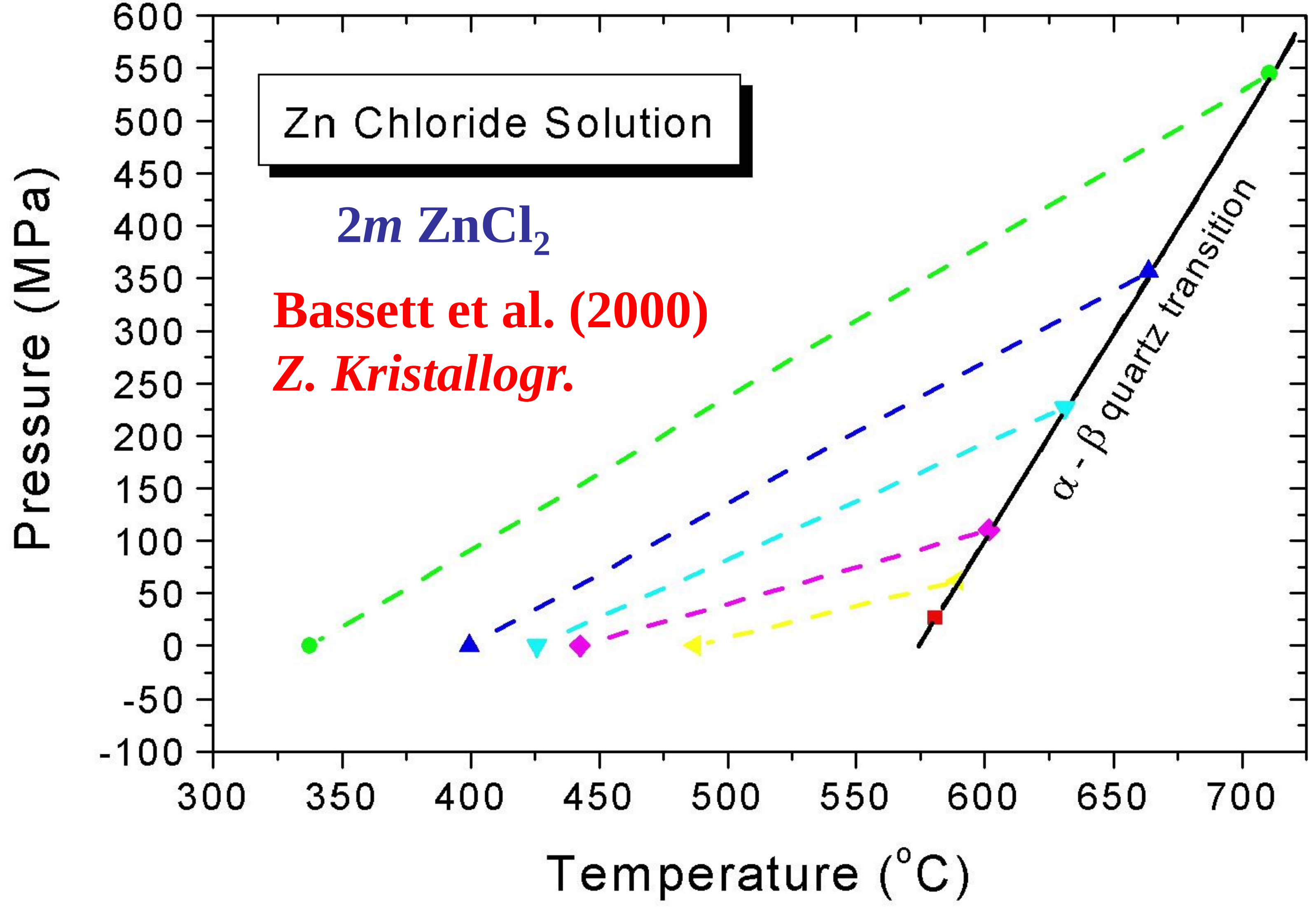
Zn Chloride Solution
2m ZnCl2
Bassett et al. (2000)
Z. Kristallogr.
Pressure (MPa)
Temperature (°C)
α - β quartz transition
600
550
500
450
400
350
300
250
200
150
100
50
0
-50
-100
300
350
400
450
500
550
600
650
700

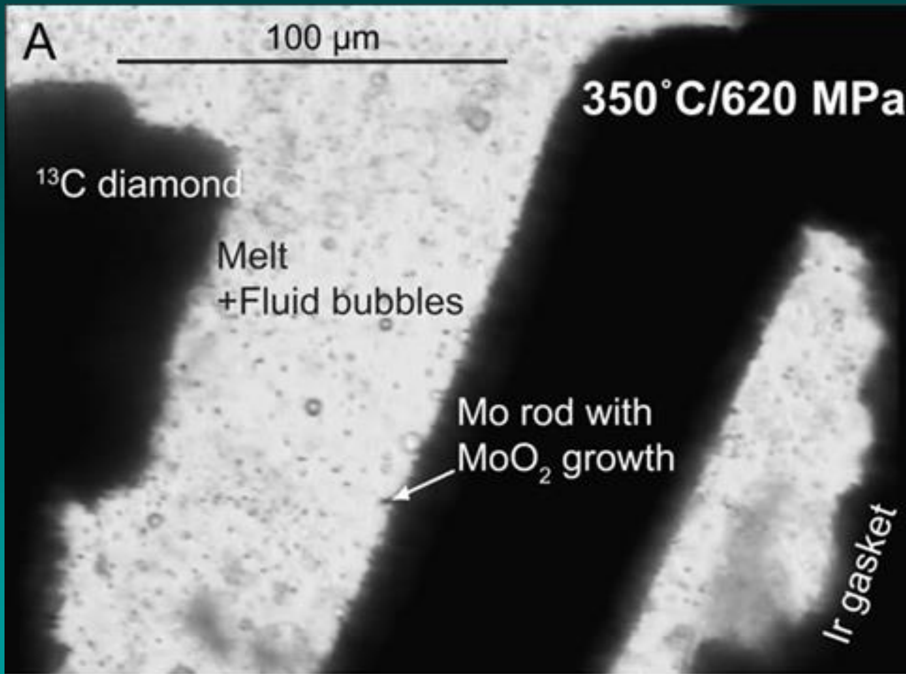
A
100 μm
350˚C/620 MPa
13C diamond
Melt
+Fluid bubbles
Mo rod with
MoO_2 growth
Ir gasket

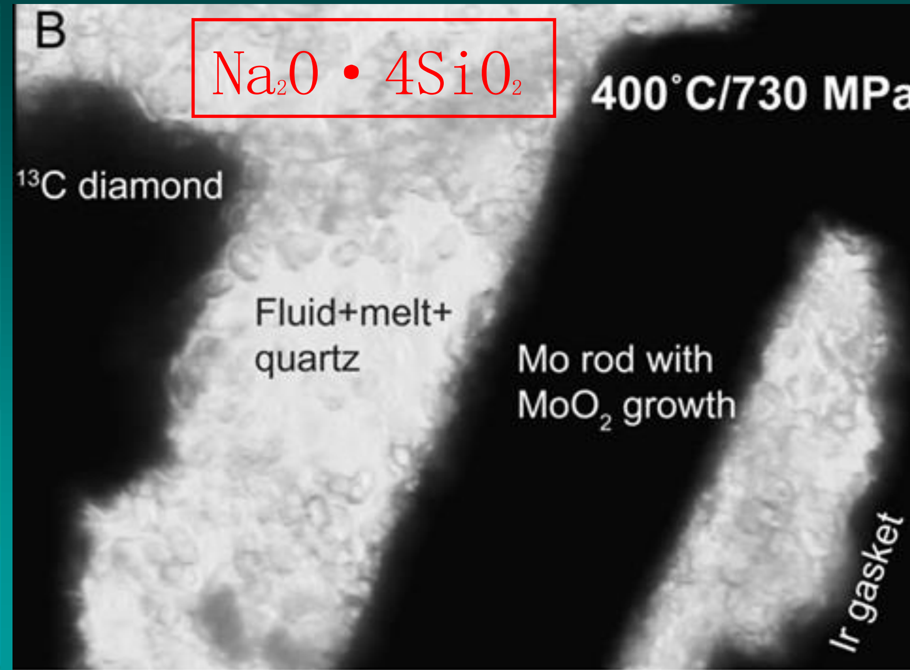
B
$Na_2O \cdot 4SiO_2$
400˚C/730 MPa
13C diamond
Fluid+melt+
quartz
Mo rod with
MoO_2 growth
Ir gasket

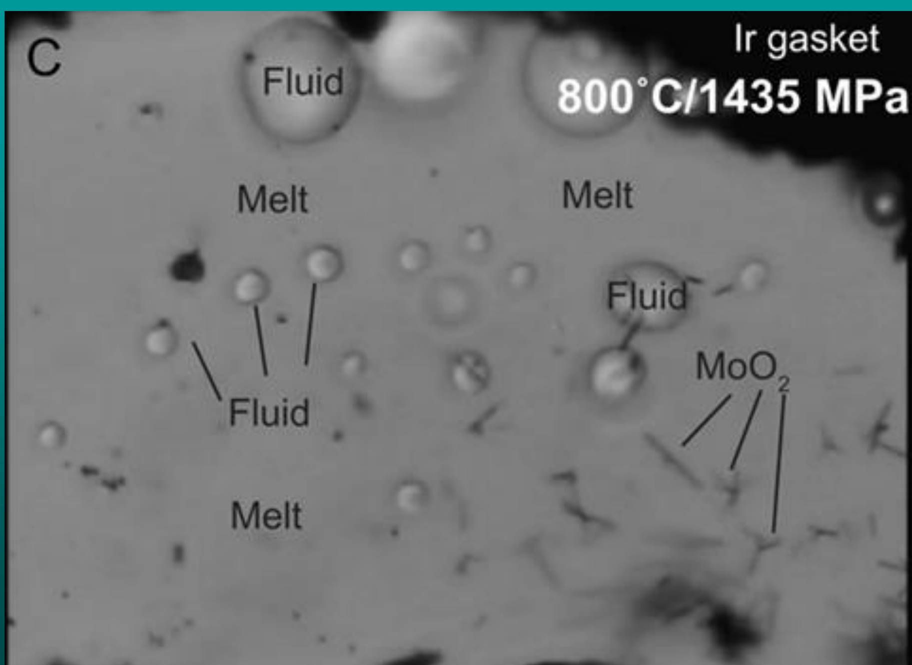
C
Ir gasket
Fluid
800˚C/1435 MPa
Melt
Melt
Fluid
MoO_2
Fluid
Melt

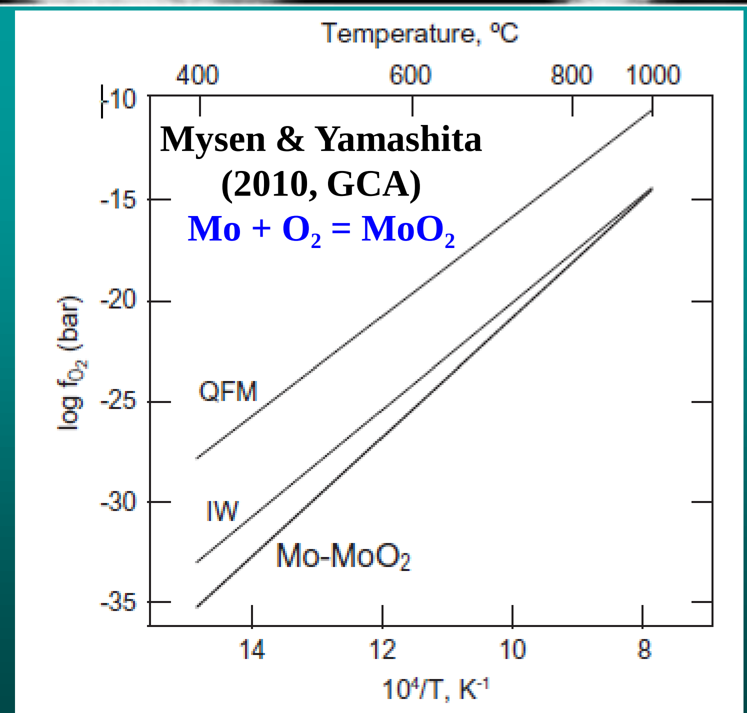
Temperature, ºC
400
600
800
1000
Mysen & Yamashita
(2010, GCA)
$Mo + O_2 = MoO_2$
log f_{O_2} (bar)
-10
-15
-20
-25
-30
-35
QFM
IW
$Mo-MoO_2$
14
12
10
8
$10^4/T$, K^{-1}


中国科学院
深海科学与工程研究所
Institute of Deep-sea Science and Engineering, CAS